











RESEARCH ARTICLE

Connectivity and molecular profiles of *Foxp2*- and *Dbx1*-lineage neurons in the accessory olfactory bulb and medial amygdala

Nandkishore Prakash¹  | Heidi Y. Matos¹  | Sonia Sebaoui¹  | Luke Tsai¹  |
 Tuyen Tran¹ | Adejimi Aromolaran¹ | Isabella Atrachji¹ | Nya Campbell¹ |
 Meredith Goodrich¹ | David Hernandez-Pineda¹ | Maria Jesus Herrero¹  |
 Tsutomu Hirata¹ | Julieta Lischinsky¹  | Wendolin Martinez¹ | Shisui Torii¹ |
 Satoshi Yamashita¹ | Hassan Hosseini²  | Katie Sokolowski¹ | Shigeyuki Esumi¹ |
 Yuka Imamura Kawasawa⁴  | Kazue Hashimoto-Torii¹ | Kevin S. Jones^{2,3}  |
 Joshua G. Corbin¹ 

¹Center for Neuroscience Research, Children's Research Institute, Children's National Hospital, Washington, District of Columbia, USA

²Department of Pharmacology, University of Michigan Medical School, Ann Arbor, Michigan, USA

³Neuroscience Graduate Program, University of Michigan Medical School, Ann Arbor, Michigan, USA

⁴Department of Pharmacology, Pennsylvania State University College of Medicine, Hershey, Pennsylvania, USA

Correspondence

Nandkishore Prakash and Joshua G. Corbin, Center for Neuroscience Research, Children's Research Institute, Children's National Hospital, 111 Michigan Avenue NW, Washington, DC 20010, USA.

Email: nprakash@childrensnational.org and JCorbin@childrensnational.org

Funding information

PNC Charitable Foundation; National Institute on Drug Abuse, Grant/Award Number: R01DA020140

Abstract

In terrestrial vertebrates, the olfactory system is divided into main (MOS) and accessory (AOS) components that process both volatile and nonvolatile cues to generate appropriate behavioral responses. While much is known regarding the molecular diversity of neurons that comprise the MOS, less is known about the AOS. Here, focusing on the vomeronasal organ (VNO), the accessory olfactory bulb (AOB), and the medial amygdala (MeA), we reveal that populations of neurons in the AOS can be molecularly subdivided based on their ongoing or prior expression of the transcription factors *Foxp2* or *Dbx1*, which delineate separate populations of GABAergic output neurons in the MeA. We show that a majority of AOB neurons that project directly to the MeA are of the *Foxp2* lineage. Using single-neuron patch-clamp electrophysiology, we further reveal that in addition to sex-specific differences across lineage, the frequency of excitatory input to MeA *Dbx1*- and *Foxp2*-lineage neurons differs between sexes. Together, this work uncovers a novel molecular diversity of AOS neurons, and lineage and sex differences in patterns of connectivity.

KEYWORDS

accessory olfactory system, *Dbx1*, *Foxp2*, medial amygdala, olfactory neuronal diversity, sex differences, vomeronasal organ

1 | INTRODUCTION

1.1 | Rodent olfactory circuitry

The olfactory system is divided into two functionally distinct components: the main olfactory system (MOS) and the accessory olfactory system (AOS). Odorants that activate the MOS bind to receptors expressed by olfactory sensory neurons (OSNs) in the main olfactory epithelium (MOE) in the nose, which projects directly to the main olfactory bulb (MOB) in the brain (Dulac & Wagner, 2006; Mombaerts et al., 1996; Vassar et al., 1994). From here, information is sent to olfactory cortical areas for higher order processing (Hintiryan et al., 2012; Igarashi et al., 2012; Shipley & Adamek, 1984). In contrast, odorants that stimulate the AOS bind directly to receptors expressed by vomeronasal sensory neurons (VSNs) in the vomeronasal organ (VNO), located in the lower part of the nasal septum in proximity to the roof of the mouth. The AOS processes both volatile and nonvolatile cues that are mainly dedicated for innate behaviors such as mating, territorial defense, and predator avoidance (Papes et al., 2010). Nonvolatile cues include pheromones, such as those released by anal and lacrimal glands and those present in urine (Cavaliere et al., 2020; Stowers & Liberles, 2016). These cues impart information regarding the hormonal state and sex of a conspecific (Ben-Shaul et al., 2010; Del Punta et al., 2002; Dulac & Wagner, 2006; Kimchi et al., 2007; Stowers et al., 2002; Thoß et al., 2019; Wysocki & Lepri, 1991). VNO OSNs project directly to the accessory olfactory bulb (AOB), which sits apart from the MOB in the posterior-dorsal aspect of the olfactory bulb (OB) (Wagner et al., 2006). The AOB projects directly to the medial (MeA) and cortical (CoA) nuclei of the amygdala and the bed nucleus of stria terminalis (BNST), all of which are interconnected and send robust projections to the hypothalamus (Davis et al., 1978; Dulac & Wagner, 2006; Dwyer et al., 2022; Gutiérrez-Castellanos et al., 2014; Lischinsky et al., 2023; Meurisse et al., 2009; Pardo-Bellver et al., 2012). The direct input from the MOB and AOB to higher order processing centers in the brain is unique to the olfactory system as all other sensory modalities (touch, taste, vision, hearing) are first relayed through the thalamus. Thus, the MOS and AOS work in parallel and in tandem to allow an animal to rapidly interpret a complex olfactory world without thalamic processing (Hintiryan et al., 2012; Igarashi et al., 2012; Kang, Baum, et al., 2011; Kang, McCarthy, et al., 2011; Murakami et al., 2005; Pro-Sistiaga et al., 2007; Shepherd, 2005; Shipley & Adamek, 1984).

1.2 | Olfactory system neuronal diversity

The diversity of olfactory cues that an animal senses in its environment is vast and complex. This is reflected in the large number of receptors—hundreds and thousands, which are present in the sensory neurons of the VNO and MOE, respectively (Buck & Axel, 1991; Dulac & Axel, 1995; Herrada & Dulac, 1997; Matsunami & Buck, 1997; Ryba & Tirindelli, 1997). The logic by which this complex sensory information is processed in the brain is currently much better understood in the MOS than the AOS. In the MOS, there appears to be regionaliza-

tion of olfactory cue identification in the MOE and subsequent sorting in the MOB. The MOE is subdivided into anatomically and molecularly distinct zones that recognize different odorant classes (Hallem & Carlson, 2006; Nara et al., 2011; Ruiz Tejada Segura et al., 2022). This segregation is maintained in the MOB, which is also subdivided based on the nature of the cue (Burton et al., 2022; Fishilevich & Vossahl, 2005; Ma et al., 2012; Oka et al., 2006; Rubin & Katz, 1999; Sakano, 2010; Wachowiak & Cohen, 2001). Based on cell morphology, anatomic localization, and physiological properties (Nagayama et al., 2014), the mitral and tufted (M/T) output neurons of the MOB are heterogeneous. More recent RNA-seq studies have uncovered a deeper level of diversity of MOB output neurons, identifying at least eight distinct molecular subtypes (Zeppilli et al., 2021). This molecular coding in the MOB appears to predict neuronal subtype-specific patterns of inputs to higher order neurons in the olfactory cortex, although this remains an area of intense investigation (Adam et al., 2014; Uchida et al., 2014).

Although less well characterized than the MOS, neurons within the VNO and AOB can also be characterized by several criteria. The VNO is subdivided into anatomically and molecularly distinct apical and basal layers, which project to the anterior (aAOB) and the posterior (pAOB) AOB, respectively (Dulac, 2000; Dulac & Axel, 1995; Herrada & Dulac, 1997; Ichikawa et al., 1994; Imamura et al., 1985; Jia & Halpern, 1996; Knöll et al., 2003; Matsunami & Buck, 1997; Ryba & Tirindelli, 1997; Sugai et al., 1999). Interestingly, the aAOB and pAOB are also molecularly distinct from each other (Huilgol et al., 2013) and may regulate different types of innate behaviors (e.g., reproductive versus aggressive) (Kumar et al., 1999; Montani et al., 2013; Nunez-Parra et al., 2011). Similar to the MOB, M/T neurons comprise the output neuronal population of the AOB. Based on morphological criteria, there appear to be at least three subtypes of AOB output neurons (Larriva-Sahd, 2008; Yonekura & Yokoi, 2008). However, the molecular diversity of both VNO and AOB output neurons remains unexplored.

In the MeA, a direct synaptic target of AOB output neurons, up to 20 different neuronal subtypes exist as characterized by their molecular and/or intrinsic electrophysiological properties (Bian, 2013; Carney et al., 2010; Chen et al., 2019; Keshavarzi et al., 2014; Lischinsky et al., 2017; Matos et al., 2020). In addition to possessing a variety of local interneuronal subtypes, the MeA comprises both excitatory and inhibitory output neurons (Bian et al., 2008; Choi et al., 2005; Wu et al., 2017). These MeA output neurons are subdivided based on their diverse morphological, electrophysiological, and/or molecular properties (Keshavarzi et al., 2014; Lischinsky et al., 2017; Matos et al., 2020), which correlate with the innate behaviors regulated by these neurons (Lischinsky et al., 2023). One criterion that defines molecular diversity in the MeA is the differential expression of transcription factors (e.g., *Otp*, *Foxp2*, and *Dbx1*) in embryonic progenitors that give rise to different MeA projection neuronal populations (Lischinsky et al., 2017). These transcription factor-defined populations express lineage-specific patterns of select sex hormone-related proteins (e.g., aromatase, estrogen, and androgen receptors) (Lischinsky et al., 2017) and ion channels (e.g., *Kv7.1*, *Kir5.1*, *Kir2.1*, *Slo2.2*) (Matos et al., 2020). This parcellation of MeA identity by molecular expression raises the question of whether other components of the interconnected AOS,

such as the VNO and AOB, are also subdivided by the expression of the same molecular identifiers.

1.3 | Sex differences in the AOS

One of the major functions of the AOS is to process information as to the reproductive state of conspecifics (Ben-Shaul et al., 2010). This information appears to be encoded differently in male and female brains. For example, cues from an estrus female elicit behavioral responses that are very different depending on whether the cue is being detected by a female or a male mouse (Yao et al., 2017). Although much remains to be understood, the first level of distinguishing between same or opposite sex cues is likely initiated in the VNO, where there are dedicated receptors for sex-specific cues (Isogai et al., 2011; Li & Dulac, 2018). Beyond this peripheral parsing of male/female cues, the processing of sex-specific information also occurs in higher order brain regions, such as the MeA and BNST (Bergan et al., 2014; Li et al., 2017; Rigney et al., 2019). However, how this information is relayed to and processed in the MeA remains an open question.

The MeA displays extensive sex differences in cell morphology, dendritic complexity, cell size, intrinsic biophysical properties, and gene expression (Cooke & Woolley, 2005; Cooke et al., 2007; Hines et al., 1992; Matos et al., 2020). Using cFos staining and in vivo neuronal population recordings, our work (Lischinsky et al., 2017) and the work of others (Bergan et al., 2014; Li et al., 2017) revealed that the MeA also displays sex differences in neuronal population responses to olfactory cues. Patch-clamp single-neuron electrophysiological and tracing studies have also revealed sex differences in patterns of inputs to the MeA. For example, neurons in the male MeA have more excitatory input than females (Billing et al., 2020; Cooke & Woolley, 2005). However, the MeA neuronal subtype target of these inputs remains unknown. Here, in addition to revealing lineage diversity in the AOS, we took advantage of our ability to specifically tag two major populations of MeA GABAergic output neurons, *Foxp2*- and *Dbx1*-lineage neurons, to further address putative sex differences in synaptic inputs. Such information is necessary to piece together a neuronal subtype-level understanding of how male and female brains differentially process olfactory information for appropriate behavioral outputs.

1.4 | Summary

The identification of neuronal diversity by transcription factors that are expressed during embryogenesis has provided a roadmap to unraveling the functionality of different neuronal subclasses across the nervous system. For example, this approach has been highly informative in elucidating the function of cortical interneurons (Batista-Brito et al., 2008; Mayer et al., 2018; Mi et al., 2018). Here, we used transcription factor expression, specifically ongoing or prior expression of *Foxp2* or *Dbx1* as an entry point to parse neuronal diversity in the AOS and further explore sex-specific patterns of input to the MeA, a main locus of convergence for olfactory cues with innate behavioral rele-

vance. Our findings also provide a platform for future exploration of the specific behavioral roles played by transcription factor-identified AOS circuits.

2 | MATERIALS AND METHODS

2.1 | Animals

Mice were housed on a 12-h light/dark cycle and had ad libitum access to food and water. All mice used here were considered adult at >2 months, with specific ages for each experiment indicated below. Mice used were *Foxp2^{cre}* (JAX #030541), *Dbx1^{cre}* (Bielle et al., 2005), C57BL/6 (JAX #000664), *LSL-FlpO* (JAX #028584), and *Rosa26YFP* (JAX# 006148). Mice were genotyped using a commercial genotyping service (Transnetyx Inc.). *Foxp2^{cre}* and *Dbx1^{cre}* mice were maintained as heterozygotes on the C57BL/6 background and crossed to *Rosa26YFP* mice as described in Section 3.

2.2 | Viruses and stereotaxic surgery

All experimental and surgical procedures were conducted in accordance with and approved by the Institutional Animal Care and Use Committee at Children's National Hospital. For all surgeries, adult (2- to 5-month-old) animals were anaesthetized with isoflurane and placed into a stereotaxic apparatus (Stoelting Co. #51600). Body temperature was maintained with a heating pad during surgery and recovery, and 1.5%–2% isoflurane was delivered continuously through a nose port. Animals were treated with analgesic buprenorphine (0.09 mg/kg body weight, of 0.03 mg/mL buprenorphine prepared in sterile saline) prior to surgery and every 12 h afterward, as needed. Mice were monitored daily and sacrificed 2–5 weeks after viral injection.

2.2.1 | Accessory olfactory bulb

Virus obtained from the University of North Carolina (UNC) Vector Core, mixed 1:1 (v/v) with blue fluorescent 1% solid polymer microspheres (Thermo Fisher Scientific, Cat#B0100), was injected unilaterally (400 nL, at 30 nL/min) into the AOB (Anterior-Posterior (AP): +4.1, Medial-Lateral (ML): ±1.0, Dorsal-Ventral (DV): –1.5 mm from Bregma) with a Hamilton syringe, into either *Foxp2^{cre}* (Virus: rAAV5-hSyn-Con/Foff.EYFP.WPRE, Titer: 2.6×10^{12} GC/mL) or *Dbx1^{cre};FlpO* (Virus: rAAV5-hSyn-Coff/Fon.EYFP.WPRE, Titer: 3.6×10^{12} GC/mL) adult mice. Following virus delivery, the syringe was left in place for 3 min to prevent backflow and then slowly withdrawn.

2.2.2 | Medial amygdala

AAV2-retro virus (Virus: rAAV2-retro-Ef1a-DO_DIO-TdTomato_EGFP-WPRE-pA, Titer: 1.0×10^{13} GC/mL), obtained from Janelia Viral Tools Facility (now Addgene Plasmid #37120, RRID: Addgene_37120), was injected bilaterally (200 nL, at 15 nL/min) into the MeA (AP: –1.6, ML: ±2.2, DV: –4.8 mm from Bregma) of adult *Foxp2^{cre}* mice.

2.3 | Immunohistochemistry

Adult animals were anaesthetized and transcardially perfused with 10 mL of 1× phosphate-buffered saline (PBS), followed by 10 mL of 4% paraformaldehyde (PFA) in 1× PBS. After perfusion, the brains were extracted and incubated overnight in the same fixative and cryoprotected in phosphate-buffered 30% sucrose solution for >48 h at 4°C. After cryoprotection, brains were embedded in O.C.T. Compound (Fisher HealthCare Cat No. 23-730-571). For experiments described in Figures 4 and 8, serial 40 to 60µm coronal cryosections of the AOB and MeA (Figure 4) or MeA alone (Figure 8) were cut using a cryostat (CM3050S, Leica) and collected in PBS containing 0.02% (w/v) sodium azide. For immunofluorescence staining in the AOB (Figure 2), 30µm-thick coronal cryosections were used and sampled every 120 µm. For experiments in Figures 2 and 4, the full antero-posterior range of the AOB (Bregma +3.56 mm to Bregma +2.96 mm) based on Franklin and Paxinos (2008) was sampled. For experiments in Figures 4 and 8, the full antero-posterior range of the MeA from Bregma –1.34 mm to Bregma –2.18 mm was sampled. Sections were excluded if found to be outside region boundaries or damaged in the region of interest. Sections were then incubated in blocking buffer (5%–10% normal donkey serum, 0.5% Triton X-100, 1× PBS) for 1 h at room temperature (RT) and subsequently incubated in the primary antibody mixture diluted in blocking buffer overnight at 4°C. Sections were then rinsed 3 × 10 min with PBST (1× PBS with 0.5% Triton X-100) and incubated in appropriate secondary antibodies for 1 h at RT. Sections were then washed 3 × 10 min with PBST and 1 × 10 min with 1× PBS, and finally mounted with Fluoromount G containing DAPI (Thermo Fisher, Cat No.0100-20).

All primary and secondary antibodies were obtained commercially (Table 1) and validated by the manufacturer or by prior studies. Immunogen information is available on the RRID portal and manufacturers' webpages. We optimized the dilutions for our assays. For primary antibodies, we further verified their staining patterns by comparing expression patterns to published literature and/or expected expression patterns from the Allen Brain Atlas (Lein et al., 2006), when available. Secondary antibodies were also routinely tested by us for specificity using negative controls without primary antibodies.

2.4 | Multiplexed fluorescent in situ hybridization

Eight-week-old male *Dbx1^{cre};RYFP* mice were transcardially perfused with 10 mL ice-cold 1× PBS, followed by 10 mL freshly prepared ice-cold 4% PFA in 1× PBS. Whole brains were collected and incubated in 4% PFA/1× PBS at 4°C for 24 h, followed by cryoprotection in 30% sucrose in 1× PBS for 48 h at 4°C. Brains were then embedded in O.C.T. Compound and stored at –80°C until cryosectioning. Ten-µm-thick slide-mounted cryosections of the MeA from Bregma –1.58 mm to Bregma –1.94 mm (as identified in Franklin & Paxinos, 2008) were obtained using a Thermo Scientific HM525 NX cryostat at –22°C. Slides were stored at –80°C with desiccant until staining. RNAscope™ HiPlex-12 Mouse kit (ACDBio, Cat #324106) was

used to detect the following *Mus musculus* mRNA targets, available from ACDBio: *Tac2* (#446391), *Tacr1* (#428781), *Trh* (#436811), *Foxp2* (#428791), *Avp* (#401391), *Ucn3* (#464861), *Npy1r* (#427021), *Htr2c* (#401001), *Npy* (#313321), *Ecel1* (#475331), and *EYFP* (#312131). Protocol for HiPlex-12 sample preparation, pretreatment, and staining was followed exactly as per ACDBio's user manual for fixed, frozen tissue sections.

2.5 | Microscopy

To analyze labeled neurons in the AOB and output projections to the MeA (Figures 3 and 4), 10× (Numerical Aperture (N.A.) 0.40) and 20× (N.A. 0.75) images were acquired using an Olympus BX63 epifluorescence microscope or a Nikon A1 confocal microscope (0.7–3.0 µm step size, 1.2 AU pinhole, 20×/N.A. 0.75 or 10×/N.A. 0.45). All off-target regions were excluded from analysis. For the synaptic labeling experiment in Figure 8, images were acquired on an Olympus FV1000 or a Nikon A1 confocal microscope. For immunofluorescence analysis in the AOB (Figure 2), images were acquired as Z-stacks (2 µm step size, 1.2 AU pinhole, 20×/N.A. 0.75 or 10×/N.A. 0.45 objectives) on a Nikon A1 confocal microscope. For RNAscope™ in situ hybridization, all samples were imaged on a Leica DMi8 THUNDER deconvolution microscope using 10× (N.A. 0.32) and 63× oil (N.A. 1.40) objectives. Excitation lines at 395, 470, 550, and 640 nm and corresponding emission filter sets (440, 510, 590, and 700 nm, respectively) were used. A camera exposure time of 20–200 ms was used for each channel, varied depending on observed signal-to-noise ratio in that channel and maintained uniformly across samples. THUNDER large-volume adaptive deconvolution with computational clearing was performed on acquired widefield images. Deconvolution settings were as follows: 1.47 refractive index, Good's roughness method of regularization with parameter 0.05, medium optimization, number of iterations and cutoff gray value set to "Auto," feature scale of 535 nm (minimum possible) for all channels except DAPI, feature length of 2673 nm (software default) for DAPI, and 98% strength for all channels. Single-Z-plane tile-scan images of the MeA were acquired with automatic linked shading correction, deconvolved, stitched (statistical blend), and exported as TIFFs for further image processing and quantification.

2.6 | Image processing, quantification, and statistical analyses

All image processing of immunohistochemistry data, including linear brightness/contrast adjustment, was performed using Fiji (Schindelin et al., 2012). For data presented in Figure 2, unilateral *Foxp2*+ neuronal counts on confocal Z-stacks were performed semiautomated, in Imaris 10.0.0 using Spots Model (estimated diameter - 3.8 µm), manually refined by quality threshold and machine learning using visual inspection, and finally filtered by "Distance to Surface" option to obtain counts within each AOB layer (which are first defined as Imaris Surface objects using boundaries demarcated in Franklin & Paxinos, 2008).

TABLE 1 List of antibodies used.

Antibody	Host species and dilution range used	Vendor and catalog no.	RRID	Immunogen	Validation
Anti-Foxp2	Rabbit, 1:500-1:1000	Atlas Antibodies, HPA000382	AB_1078908	Recombinant Protein Epitope Signature Tag (PREST) antigen sequence (from human FOXP2) Human antigen and its mouse ortholog (ENSMUSG00000029563) have 99% sequence identity	By manufacturer: Affinity purified using PREST antigen as affinity ligand Reacts with a band of approximately 100 kDa in western blot using lysates of Human Cell Line RH-30. In previous literature: Human Protein Atlas: https://www.proteinatlas.org/ENSG00000128573-FOXP2 (Enard et al., 2009; Kast et al., 2019; Kondabolu et al., 2023; Reimers-Kipping et al., 2011) By authors: Positive controls in wildtype adult mouse brains—staining pattern compared to known expression pattern of Foxp2 in other brain regions, reported previously in the literature (Co et al., 2020; Druart et al., 2020; Kast et al., 2019; Lischinsky et al., 2017, 2023).
Anti-Foxp2	Goat, 1:200	Santa Cruz Biotechnology, sc-21069	AB_2107124	Human FOXP2 N-terminus	In previous literature: (French et al., 2007; Lischinsky et al., 2017; Reimers-Kipping et al., 2011) French et al. (2007) demonstrate antibody reactivity with a band between 100 and 70 kDa in western blot using striatal precursor lysates from E16.5 mouse embryos and further validate the antibody using lysates from a conditional Foxp2 knockout that shows no band. Reimers-Kipping et al. (2011) compare results between this and the above (HPA000382, Atlas) antibody using IHC—fluorescence in adult and embryonic mouse brain.
Anti-GFP (to detect EGFP and EYFP)	Rat, 1:500-1:1000	Nacalai-Tesque, 04404-84	AB_10013361	His-GFP (full length) fusion protein	In previous literature: (Lischinsky et al., 2023; Liu et al., 2021; Nakamura et al., 2021) By authors: Positive controls—staining pattern compared to known expression pattern of Foxp2- and Dbx1- derived neurons in the wildtype adult mouse brain and vomeronasal organ, reported previously in the literature (Causeur et al., 2023; Lischinsky et al., 2017, 2023). Internal negative controls using the uninjected hemisphere in viral transduction experiments with retro-AAV2 dual-switch reporter virus show no signal or background, in contrast to strong signal on the injected side, confirming specificity.
Anti-CART	Rabbit, 1:500	Phoenix Pharmaceutical, H003-62	AB_2313614	Not available	In previous literature: (Fenwick et al., 2006; Kirouac et al., 2006; Lee et al., 2020)

(Continues)

TABLE 1 (Continued)

Antibody	Host species and dilution range used	Vendor and catalog no.	RRID	Immunogen	Validation
Anti-PDE4A	Rabbit, 1:500	Abcam, ab14607	AB_301375	C-terminal region of Human PDE4A As per manufacturer: Labels all known PDE4A variants (A1, A5, A8, Ax, and testis-specific A).	By manufacturer: Immunogen affinity purified In previous literature: (Katrancha et al., 2019; Münch et al., 2018; Yang et al., 2018)
Anti-OMP	Goat, 1:5000	Wako, 544-10001	AB_2315007	Rodent OMP	In previous literature: (Henkel et al., 2017; Nguyen & Imamura, 2019; Treloar et al., 1999)
Anti-PSD95	Rabbit, 1:50	Proteintech, 20665-1-AP	AB_2687961	Peptide	By manufacturer: Antigen affinity purified Western blot analysis using HeLa cell lysates shows reactivity with a single band of size between 70 and 100 kDa that is absent when using HeLa cell lysates pretransfected with shRNA directed against PSD95. Positive controls for immunohistochemistry using paraffin embedded mouse and rat brain slices demonstrate strong, specific staining in the dentate gyrus with protein localized near cell surface as expected from known function at synapses. In previous literature: (Chen et al., 2016; Li et al., 2021; Wang et al., 2021)
Anti-VGLUT2	Guinea Pig, 1:100	Millipore, AB2251-1	AB_2665454	KLH-conjugated linear peptide corresponding to 18 amino acids from the C-terminal, cytoplasmic domain of rat Vesicular Glutamate Transporter 2 (VGLUT2)	By manufacturer: Unpurified. Representative lot data show western blot reactivity with a band of approximate size 56 kDa in rat brain membrane extract, smaller than calculated size of 64.6 kDa consistent with reported apparent molecular weight. Representative lot data show punctate, cytoplasmic staining in mouse and rat formalin-fixed paraffin-embedded brain tissue section. In previous literature: (Li et al., 2020; Madeira et al., 2020; Modol et al., 2020) Li et al. (2020) use shRNA approach to knockdown VGLUT2 and demonstrate consequent lack of immunoreactivity.

(Continues)

TABLE 1 (Continued)

Antibody	Host species and dilution range used	Vendor and catalog no.	RRID	Immunogen	Validation
Anti-Gephyrin	Rabbit, 1:200	Thermo Fisher, PA5-55157	AB_2641960	Recombinant protein corresponding to human Gephyrin, amino acids 291–430 100% sequence identity with mouse ortholog	By manufacturer: Affinity purified using antigen Western blot analysis of PC-3 cell lysates demonstrates reactivity with a single band of approximately 93 kDa, which is nearly absent in lysates of PC-3 cells transfected with shRNA directed against GPHN. Immunohistochemistry shows significant staining in human cerebral cortex and weak or minimal staining in human lymph node concordant with RNA-Seq TPM values in the two tissues. In previous literature: Not available
Anti-VGAT	Mouse, 1:1000	Invitrogen, MA5-24643	AB_2637258	Recombinant protein corresponding to human VGAT amino acids 13–103 95% sequence identity to mouse ortholog	By manufacturer: Immunohistochemistry in mouse and rat brain slices demonstrates VGAT immunoreactivity in brain regions known to have GABAergic neurons, for example, substantia nigra pars reticulata, cerebellum, and globus pallidus. In previous literature: (Kaczmarek-Hajek et al., 2018; Sammoura et al., 2023; Torz et al., 2022)
Anti-tdTomato	Goat, 1:500	LSBio, LS-C340696	AB_2819022	Purified recombinant peptide (<i>Discosoma</i> tdTomato) produced in <i>E. coli</i>	By manufacturer: Immunoaffinity purified Western blot analysis of HEK293 cell lysates shows reactivity with a single 55-kDa band Does not cross-react with GFP In previous literature: (Beier et al., 2021; Co et al., 2020; Zhang et al., 2021) By authors: Internal negative controls using the uninjected hemisphere in viral transduction experiments with retro-AAV2 dual-switch reporter virus show no signal or background, in contrast to strong signal on the injected side, confirming specificity.
Anti-Rabbit secondary (Cy3-conjugated)	Donkey, 1:1000	Jackson ImmunoResearch, 711-165-152	AB_2307443	Rabbit IgG (H+L)	Negative control by authors with identical immunohistochemistry conditions but no primary antibody shows no discernible background staining.
Anti-Rabbit secondary (Cy5-conjugated)	Donkey, 1:1000	Jackson ImmunoResearch, 711-175-152	AB_2340607	Rabbit IgG (H+L)	Negative control by authors with identical immunohistochemistry conditions but no primary antibody shows no discernible background staining.

(Continues)

TABLE 1 (Continued)

Antibody	Host species and dilution range used	Vendor and catalog no.	RRID	Immunogen	Validation
Anti-Rat secondary (Alexa Fluor 488 conjugated)	Donkey, 1:500-1:1000	Thermo Fisher Scientific, A-21208	AB_2535794	Rat IgG (H+L)	Negative control by authors with identical immunohistochemistry conditions but no primary antibody shows no discernible background staining.
Anti-Mouse secondary (Cy3-conjugated)	Donkey, 1:1000	Jackson ImmunoResearch, 711-165-150	AB_2340813	Mouse IgG (H+L)	Negative control by authors with identical immunohistochemistry conditions but no primary antibody shows no discernible background staining.
Anti-Mouse secondary (Cy5-conjugated)	Donkey, 1:1000	Jackson ImmunoResearch, 715-175-150	AB2340819	Mouse IgG (H+L)	Negative control by authors with identical immunohistochemistry conditions but no primary antibody shows no discernible background staining.
Anti-Goat secondary (Cy3-conjugated)	Donkey, 1:1000-1:1500	Jackson ImmunoResearch, 705-165-147	AB_2307351	Goat IgG (H+L)	Negative control by authors with identical immunohistochemistry conditions but no primary antibody shows no discernible background staining.
Anti-Goat secondary (Cy5-conjugated)	Donkey, 1:1000	Jackson ImmunoResearch, 705-175-147	AB_2340415	Goat IgG (H+L)	Negative control by authors with identical immunohistochemistry conditions but no primary antibody shows no discernible background staining.
Anti-Guinea Pig secondary (Cy3-conjugated)	Donkey, 1:1000	Jackson ImmunoResearch, 706-165-148	AB_2340460	Guinea Pig IgG (H+L)	Negative control by authors with identical immunohistochemistry conditions but no primary antibody shows no discernible background staining.
Anti-Guinea Pig secondary (Alexa Fluor 647-conjugated)	Donkey, 1:1000	Jackson ImmunoResearch, 706-605-148	AB_2340476	Guinea Pig IgG (H+L)	Negative control by authors with identical immunohistochemistry conditions but no primary antibody shows no discernible background staining.

Accuracy of semiautomated counting was verified by comparison to manual counting of 25% of the data set in Fiji. Unilateral *Dbx1* (EYFP) and co-expression counts were performed manually. For *Foxp2* and EYFP, a neuron was counted only if it also had a visible DAPI+ nucleus. Data were first sorted according to antero-posterior position by visual inspection and comparison to Franklin and Paxinos (2008), and then quantified by AOB layer (absolute neuron counts), also following the layer nomenclature used by Franklin and Paxinos (2008) and previously published studies (Cádiz-Moretti et al., 2014; Gascuel et al., 2012; Gentier et al., 2015; Kuteeva et al., 2004; Stanic et al., 2006). The glomerular layer (GIA) was identified by its distinctive clustering of cell bodies in middle and posterior AOB sections. The external plexiform layer (EplA) was identified in middle AOB sections as a distinct region (band) of sparseness in cell bodies immediately ventral to the GIA and dorsal to the mitral cell layer (MiA). The MiA in middle AOB sections was demarcated as the AOB layer immediately dorsal to the dorsal lateral olfactory tract (dlo), and it has a visibly denser cell body distribution and is thicker than the EplA. In anterior AOB sections, the GIA is entirely absent, the MiA was first demarcated as the crescent-shaped region dorsal to the dlo, with a thick, dense distribution of cell bodies and the EplA as the remainder of the AOB. In posterior AOB sections, the EplA and MiA are visually indistinguishable and were consequently considered together as a single sublayer (the MiA). All counts were analyzed in GraphPad Prism 9 using independent Mann–Whitney *U* tests ($\alpha = .05$) with number of unilateral sections as sample size and without correction for multiple comparisons. Percentages reported in Figures 1 and 4 were calculated by averaging individual percentages obtained from each datapoint (individual mouse) within an experimental group, whereas the absolute numbers reported in the text in parentheses are summations of individual cell counts obtained from all datapoints (all mice) within an experimental group. For in situ hybridization data, linear brightness/contrast adjustments were made for all channels in Fiji similarly across tissue sections; regions of interest for the MeA were drawn based on Franklin and Paxinos (2008) using a 10 \times tile-scanned DAPI image of the whole section; and counting labels were added to *Foxp2* mRNA+ and EYFP mRNA+ neurons (DAPI+ nuclei with at least six mRNA puncta on or clustered tightly around nucleus) in the MeA using the Cell Counter plugin. These were aligned individually to images of each investigated mRNA target using DAPI channel for transparency-based manual image registration in Adobe Photoshop. MeA neurons expressing each target (six or more mRNA puncta on or tightly clustered around nucleus) were quantified within *Foxp2* mRNA+ and EYFP mRNA+ neurons and statistically analyzed (Mann–Whitney *U* tests, $\alpha = 0.05$, followed by false discovery rate [FDR] correction for multiple comparisons using Benjamini–Hochberg procedure with 10% FDR) and plotted using GraphPad Prism 9.

2.7 | Patch-clamp electrophysiology recordings

Sexually naive, adult mice aged Postnatal day 50 to Postnatal day 90 were deeply anaesthetized with isoflurane and sacrificed. Brains were removed and immediately immersed in an ice-cold carbogenated

(95% O₂ and 5% CO₂) sectioning solution (75 mM sucrose, 10 mM D-glucose, 25 mM NaHCO₃, 87 mM NaCl, 2.5 mM KCl, 1.0 mM NaH₂PO₄, 1.0 mM MgCl₂, and 0.5 mM CaCl₂; pH 7.3; 295–300 mOsm/kg). Coronal slices of 300 μ m were sectioned on a vibratome (Leica VT1200S) at the level of posterior MeA (Bregma -1.56 to -1.94 mm; Franklin & Paxinos, 1997). Slices were collected and placed in oxygen-equilibrated artificial cerebrospinal fluid (ACSF) composed of the following: 125.0 mM NaCl, 3.5 mM KCl, 1.0 mM MgCl₂, 1.25 mM NaH₂PO₄, 2.0 mM CaCl₂, 26.0 mM NaHCO₃, and 10.0 mM D-glucose; pH 7.3; 295–300 mOsm/kg. *Dbx1*^{cre};RYFP-positive or *Foxp2*^{cre};RYFP-positive neurons were visualized using a Nikon FN1 epifluorescence microscope with a 450 to 490 nm filter. Whole-cell patch-clamp recordings from EYFP-positive fluorescent neurons were performed at RT with continuous perfusion of carbogenated ACSF. Signals were acquired on a patch-clamp amplifier (Multiclamp 200B) and digitized at 250 kHz with an A/D converter (DigiDATA1550B). Recordings were performed with glass electrodes pulled on a Sutter P-2000 pipette puller (Sutter Instruments), with 3–5 M Ω resistance, and filled with a potassium gluconate-based intracellular solution containing the following: 119.0 mM K-gluconate, 2.0 mM Na-gluconate, 6.0 mM NaCl, 2.0 mM MgCl₂, 10.0 mM HEPES, 0.9 mM EGTA, 4.0 mM Mg-ATP, 14.0 mM Tris-creatine PO₄, and 0.3 mM Tris-GTP; pH 7.3; 285–295 mOsm/kg. Neurons were first recorded in current clamp configuration as reported in Matos et al. (2020). Subsequently, they were switched from current clamp to voltage clamp configuration. Each seal was tested to have maintained access resistance at <30 M Ω throughout the current and voltage clamp recordings, verified at the beginning and end of a recording session. Neurons that did not meet these criteria were excluded from all experiments. Voltage clamp recordings were done for 3 min at a gap-free holding potential of -60 mV. Only the third minute of recording for each stage was analyzed. sEPSC events were detected using Clampfit Software 10.7 (Molecular Devices) by employing “template search”—several events were initially selected and saved as a template and then used to detect similar events from the entire recording. Statistical analysis and plotting of event frequency data were performed in GraphPad Prism 9. Data were determined to have a lognormal distribution using D’Agostino–Pearson’s test and then log-transformed for subsequent analyses with a two-way ANOVA using sex and lineage as independent variables. Homoscedasticity and normality of residuals of log-transformed data were verified by Spearman’s test and D’Agostino–Pearson omnibus (K^2) tests, respectively. ANOVA interaction and main effects were inspected ($\alpha = .05$) using *F* test, followed by Sidak’s test for multiple pairwise planned comparisons with $\alpha = .05$.

3 | RESULTS

3.1 | *Foxp2*+ and *Dbx1*-lineage neurons in the VNO and AOB

Our previous studies revealed that *Foxp2*+ and *Dbx1*-lineage neurons comprise nonoverlapping populations of inhibitory output

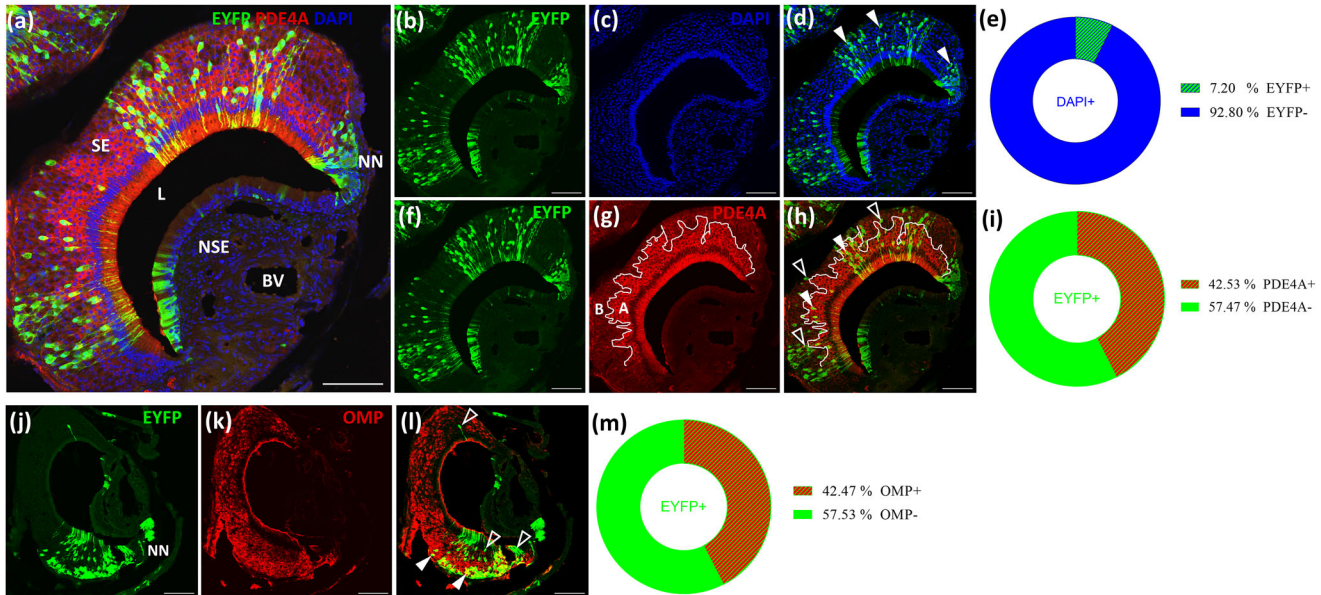


FIGURE 1 *Dbx1*-lineage chemosensory neurons in the vomeronasal organ (VNO). (a) Triple immunofluorescence for EYFP (green), PDE4A (red), and DAPI (blue) in a unilateral coronal section of the VNO from a *Dbx1^{cre};RYFP* mouse. Panels (b–d) and (f–h) correspond to the image shown in panel (a). (b–d) Recombined EYFP+ neurons (green) are shown within the total DAPI+ (blue) population across the sensory epithelium (SE). Solid white arrowheads in panel (d) highlight EYFP+ neurons. (e) Quantification of EYFP+ neuron number as a percentage of the total DAPI+ population. (f–h) EYFP+ neurons are observed in both the PDE4A+ apical layer (A) and the PDE4A- basal layer (B), demarcated by the white lines in panels (g) and (h). Solid white arrowheads in panel (h) highlight EYFP+ PDE4A+ neurons (yellow) in the apical VNO. Empty white triangles highlight EYFP+ PDE4A- neurons (green) in the basal VNO. (i) Quantification of the proportions of PDE4A+ (apical) and PDE4A- (basal) neurons within the EYFP+ (*Dbx1*-lineage) population. (j–l) Double immunofluorescence for EYFP (green, j) and OMP (red, k), a marker of mature olfactory neurons. Solid white arrowheads in panel (l) highlight EYFP+ OMP+ (yellow) mature *Dbx1*-lineage neurons and empty white triangles highlight EYFP+ OMP- (green) immature *Dbx1*-lineage neurons in the neurogenic niche. (m) Quantification of mature EYFP+ neuron number as a percentage of the total EYFP+ population. $n = 18$ mice (9 males and 9 females, 4–6 unilateral sections/mouse) in panels (e), (i), and (m). BV, blood vessel; L, lumen; NN, neurogenic niche; NSE, nonsensory epithelium; SE, sensory epithelium. Scale bars equal 100 μm .

neurons in the MeA (Lischinsky et al., 2017, 2023). In the MeA, *Foxp2* is first expressed during embryogenesis and continues throughout adulthood. In contrast, *Dbx1* is expressed only during embryogenesis in mitotic forebrain ventricular zone progenitors and is turned off when they transition to the subventricular zone (Hirata et al., 2009). To mark *Dbx1*-lineage neurons, we used an anti-GFP antibody on tissue from previously validated (Bielle et al., 2005) *Dbx1^{cre}* mice crossed to *RYFP* reporter mice (Figures 1, 2, 5, 6, and 7). For gene expression studies (Figures 2, 5, and 6), where we assessed both *Dbx1*-lineage and *Foxp2*+ neurons, *Foxp2*+ neurons were identified using a well-characterized antibody or by RNAscope™ in situ hybridization. For viral cre-based connectivity tracing, electrophysiology, and synaptic experiments (Figures 3, 4, 7, and 8), we used previously validated *Foxp2^{cre}* mice (Roussou et al., 2016) crossed to *RYFP* reporter mice or injected with an *EYFP*- and/or *tdTomato*-carrying reporter virus.

We first determined if *Foxp2*+ or *Dbx1*-lineage neurons are present in the VNO (Figure 1) and AOB (Figure 2) of 1- to 3-month-old mice. The adult VNO contains mature vomeronasal neurons (VSNs) and immature newly generated VSNs in a neurogenic niche located at the edge of the VNO (Katreddi & Forni, 2021). While no *Foxp2*+ neurons were found in the adult VNO (data not shown), we observed numerous *Dbx1*-lineage neurons, comprising ~7% of the total DAPI+

population (5589 EYFP+ neurons out of 78,382 DAPI+ cells) across the VNO sensory epithelium (Figure 1a–e). The adult VNO comprises a lumen-facing apical layer and a non-lumen-facing basal layer. These layers project to the anterior and posterior AOB, respectively (Jia & Halpern, 1996; Knöll et al., 2003; Sugai et al., 1999). The apical layer is marked by PDE4A, a member of the cAMP-specific family of phosphodiesterases (Lau & Cherry, 2000). We found *Dbx1*-lineage VSN cell bodies almost evenly distributed across the PDE4A+ (~43%, 2496 PDE4A+ neurons out of 5589 EYFP+ neurons) apical layer and the PDE4A- (~57%, 3093 PDE4A- neurons out of 5589 EYFP+ neurons) basal layer (Figure 1a,f–i). Co-labeling of EYFP+ neurons with OMP, a marker for mature VNO neurons (Farbman & Margolis, 1980), revealed that ~42% of *Dbx1*-lineage neurons are mature (2174 OMP+ neurons out of 5589 EYFP+ neurons; Figure 1j–m). Thus, in the VNO, *Dbx1*-lineage neurons comprise both immature and mature VSNs located in both the apical and basal layers.

In the OB, we next examined if *Foxp2*+ and *Dbx1*-lineage neurons were present in the MOB and AOB. Co-immunostaining for *Foxp2* and EYFP in *Dbx1^{cre};RYFP* mice revealed neurons from both populations across the OB (Figure 2a,h,p), with an apparent greater number of *Foxp2*+ neurons. Focusing on the AOB, which receives direct input from the VNO, we observed *Foxp2*+ and *Dbx1*-lineage neurons located within the glomerular (GIA), external plexiform (EplA), and mitral cell

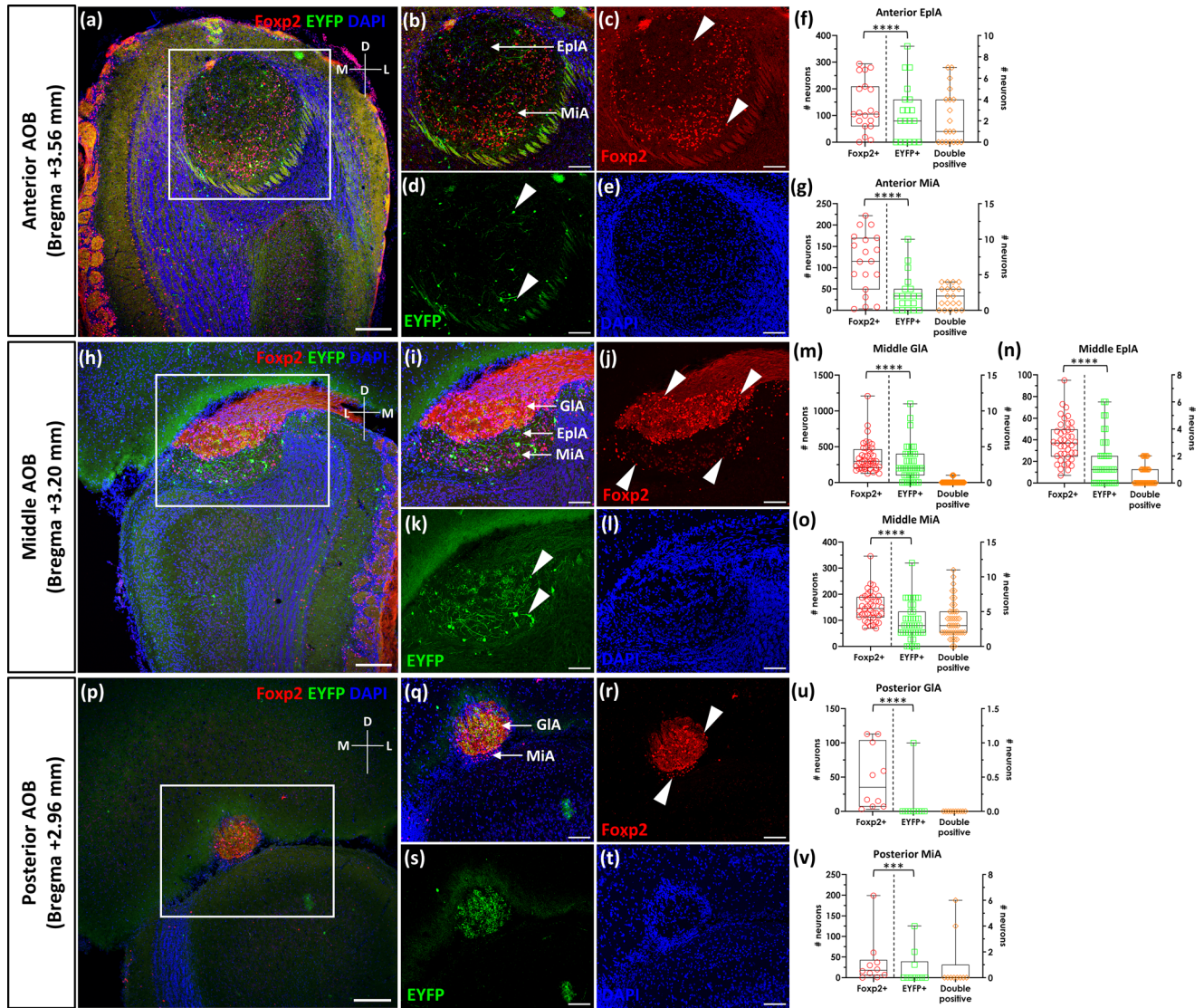


FIGURE 2 *Dbx1*-lineage and *Foxp2*+ neurons in the accessory olfactory bulb (AOB). (a, h, p) Low-magnification images of unilateral, coronal sections from the anterior (a), middle (h), and posterior (p) olfactory bulb (OB) from a *Dbx1^{Cre};RYFP* mouse. *Foxp2*+ (red) and *EYFP*+ (green, *Dbx1*-lineage) neurons identified by immunofluorescence and co-labeled with DAPI (blue). White boxes in panels (a), (h), and (p) highlight the AOB, shown at higher magnification in panels (b–e), (i–l), and (q–t). (b–e) Higher magnification images of boxed region in panel (a) show *Foxp2*+ neurons (red, c) and *EYFP*+ *Dbx1*-lineage neurons (green, d), in both the external plexiform (EplA) and mitral cell (MiA) layers of the anterior AOB. DAPI (blue) shown in panel (e). Many *Foxp2*+ neurons (red) are present throughout the AOB, with fewer *Dbx1*-lineage neurons (green, *EYFP*+). Merged image (b) shows minimal overlap of the two populations. (f, g) Box-and-whisker plots quantifying number, per unilateral section of *Foxp2*+ (red circles, left Y-axis), *EYFP*+ (green squares, right Y-axis), and co-expressing (double positive, orange diamonds, right Y-axis) neurons in the EplA (f) and MiA (g). $n = 19$ unilateral sections from five adult mice (four males, one female). (i–l) Higher magnification images of the middle AOB (boxed region in h). (i) Glomerular layer (GIA), EplA, and MiA of the AOB are shown. (m–o) Quantification of neuron number in each layer of the middle AOB. $n = 41$ unilateral sections from five adult mice (four males, one female). (q–t) Higher magnification images of the posterior AOB (boxed region in p). GIA and MiA are much smaller and the EplA is absent at the posterior level of the AOB. Quantification of each layer in the posterior AOB layer is shown in panels (u) and (v). $n = 10$ unilateral sections from five adult mice (four males, one female). Solid white arrowheads in panels (c), (d), (j), (k), and (r) highlight examples of quantified neurons. In panels (a), (h), and (p), crosses indicate section orientation (D, dorsal; M, medial; L, lateral). EplA, external plexiform layer of the AOB; GIA, glomerular layer of the AOB; MiA, mitral cell layer of the AOB. Scale bars in panels (a), (h), and (p) equal $200\ \mu\text{m}$ and in panels (b–t) $100\ \mu\text{m}$. **** $p < .001$; **** $p < .0001$ (Mann–Whitney *U* tests).

(MiA) layers (Figure 2b–g,i–o,q–v). Across all layers and the antero-posterior extent of the AOB, we found that *Foxp2*+ neurons were a greater population than *Dbx1*-lineage neurons (Figure 2f–g,m–o,u–v). We further found that in all layers, the majority of *Foxp2*+ and

Dbx1-lineage neurons were separate populations with minimal overlap in expression (Figure 2f–g,m–o,u–v), a population segregation that mimics what we previously observed in the MeA (Lischinsky et al., 2017).

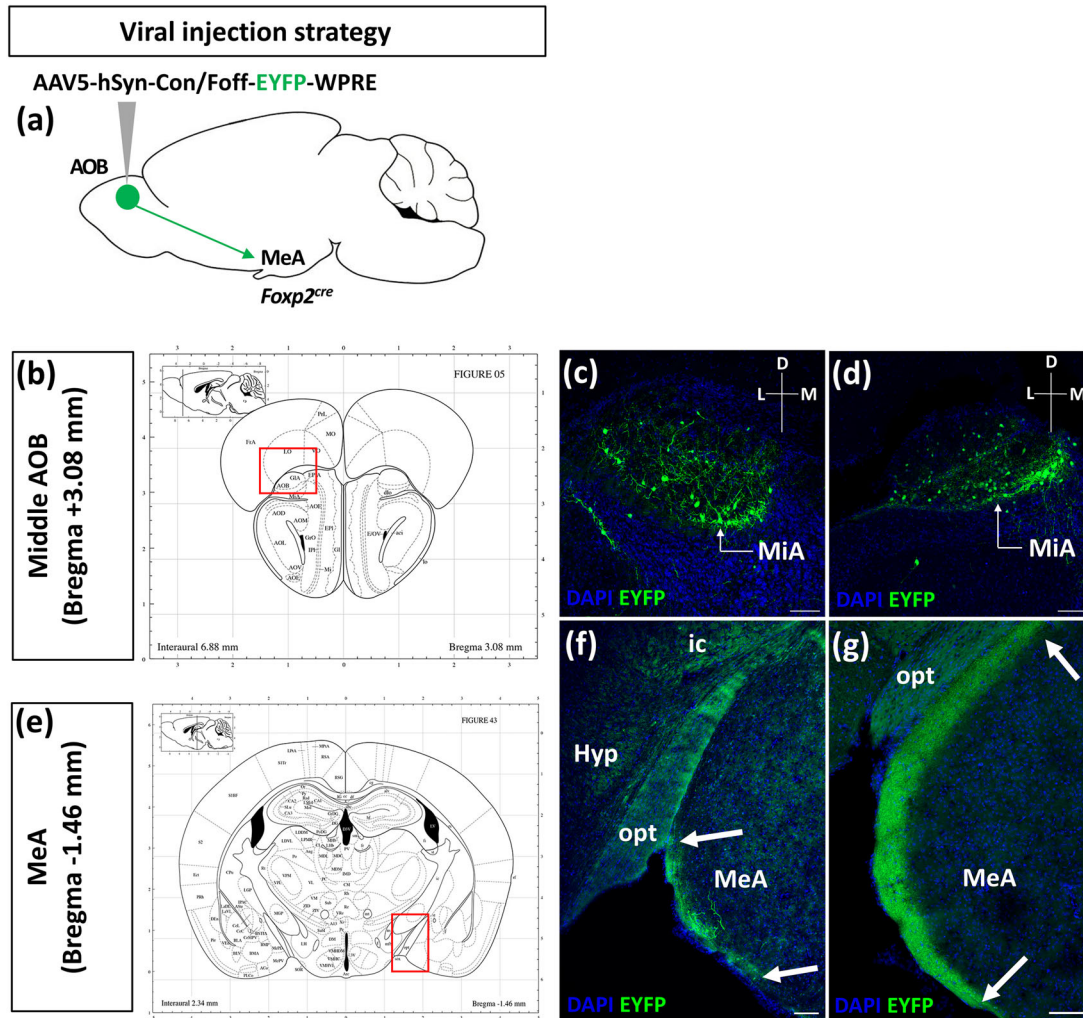


FIGURE 3 AOB *Foxp2*-lineage neurons project to the medial amygdala (MeA). (a) Schematic of anterograde viral transduction into the AOB of *Foxp2^{cre}* mice. Boxed regions within images (b, e) from Franklin and Paxinos (2008) denote the AOB and MeA shown in panels (c, d) and (f, g), respectively. (c, d) Representative images from unilateral coronal sections of virally transduced AOBs show recombinant EYFP⁺ neurons (green) from two different mice (c, d) in the AOB (middle level, Bregma +3.08 mm). (f, g) EYFP⁺ green fibers (white arrows) emanating from transduced AOB mitral cells (MiA) are observed along the input pathway to the posterior MeA (Bregma –1.46 mm)—ventral tissue boundary of the posterior MeA. Crosses in panels (c) and (d) indicate section orientation (D, dorsal; M, medial; L, lateral). AOB, accessory olfactory bulb; Hyp, hypothalamus; ic, internal capsule; MeA, medial amygdala; MiA, mitral cell layer of the AOB; opt, optic tract. In all panels, scale bar equals 100 μ m and DAPI-labelled nuclei are shown in blue. $n = 6$ mice (3 females and 3 males).

3.2 | *Foxp2*⁺ neurons comprise the majority of MeA-projecting AOB output neurons

The MeA receives direct projections from the AOB (Zheng et al., 2020). We therefore wanted to examine whether *Foxp2*- and *Dbx1*-lineage neurons in the AOB project to the MeA. To accomplish this, we injected an anterograde AAV5-*hSyn-Con/Foff.EYFP.WPRE* virus into the AOB of *Foxp2^{cre}* mice (Figure 3a) and an anterograde AAV5-*hSyn-Coff/Fon.EYFP.WPRE* virus into *Dbx1^{cre};FlpO* mice. The use of *Dbx1^{cre};FlpO* mice to trace *Dbx1*-lineage neurons is necessitated by the fact that *cre* is no longer expressed when *Dbx1* expression ceases during later embryogenesis (Bielle et al., 2005; Hirata et al., 2009; Medina et al., 2005). Constitutive *flp* expression after *cre*-driven recombination in *Dbx1^{cre};FlpO* mice enables tracing using *Flp*-dependent

reporters. Viral transduction of AAV5-*hSyn-Coff/Fon.EYFP.WPRE* in *Dbx1^{cre};FlpO* mice resulted in recombination in very few *Dbx1*-lineage neurons, thus precluding our ability to follow their projections (data not shown). This low number of recombinant AOB neurons is likely a reflection of the lower number of *Dbx1*-lineage M/T neurons compared to the number of *Foxp2*⁺ neurons (Figure 2). In contrast, in injected *Foxp2^{cre}* mice, we observed large numbers of recombinant AOB neurons (Figure 3b–d), with robust EYFP⁺ projections emanating from the AOB to the MeA (Figure 3e–g).

As we observed strong projections from *Foxp2*-lineage AOB M/T neurons to the MeA, we next wanted to determine if this population represented most of the projections to the MeA. To accomplish this, we targeted the MeA of *Foxp2^{cre}* mice with a retrograde dual-switch reporter “Retro-AAV2” virus (*rAAV2-retro-Ef1a-DO-DIO*-

TdTomato_EGFP-WPRE-pA (Saunders et al., 2012; Tervo et al., 2016) (Figure 4a,b). In addition to the MeA, we also typically observed a low level of recombination in the adjacent cortical (CoA) and posterior (PA) nuclei of the amygdala due to viral spread. Retro-AAV2 is taken up by presynaptic neuronal terminals and translocated retrogradely to cell bodies where presynaptic cre-expressing cell bodies are EGFP+/tdTomato-, while cre-negative cell bodies are EGFP-/tdTomato+ (Figure 4b). In the AOB, we found both EGFP+ and tdTomato+ neurons (Figure 4c-h) indicating that both Foxp2+ and Foxp2- AOB M/T neurons project to the amygdala. Quantification of the numbers of EGFP+ and tdTomato+ neurons revealed that the EGFP+ population represented the majority of recombined neurons (2324 EGFP+ neurons out of 3426 EGFP+ or tdTomato+ neurons; Figure 4i). We observed a few neurons expressing both EGFP and tdTomato, likely representing a low level of cre-independent background recombination reported by Tervo et al. (2016). Overall, these results indicated that in the AOB, a majority of amygdala-projecting neurons are of the *Foxp2* lineage.

This raises an intriguing question about the relative contribution of *Dbx1*-lineage versus non-*Dbx1*-lineage neurons to the output projections from the AOB to the MeA. Retrograde tracing of the *Dbx1* lineage from the MeA in adults is, however, currently precluded by the lack of a Flp-dependent version of the dual-switch retrograde AAV tracer virus.

3.3 | MeA *Foxp2*+ and *Dbx1*-lineage neurons express different cohorts of neuropeptides

Our previous studies revealed that MeA *Foxp2*+ and *Dbx1*-lineage neurons express different sex hormone-related proteins and ion channels (Lischinsky et al., 2017; Matos et al., 2020). Furthermore, a recent study has revealed that these lineages control different innate behaviors (Lischinsky et al., 2023). The MeA also expresses a variety of neuropeptides and receptors that likely play a neuromodulatory role in regulating innate behaviors such as mating, aggression, feeding, maternal care, and social interaction, based on their known roles in other limbic nuclei. To explore whether the two populations of our interest express different combinations of neuropeptides, we conducted immunohistochemistry (Figure 5) and multiplexed RNAscope™ in situ hybridization (Figure 6) in sections from *Dbx1^{cre};RYFP* mice. Candidates were chosen based on the following criteria: The gene of interest (1) is expressed in the MeA as shown either in prior published studies or the Allen Brain gene expression atlas (Lein et al., 2006), (2) plays a known role in MeA function or innate social behavior, and/or (3) was observed in a previous RNA-seq screen of the adult MeA (Chen et al., 2019). Following these criteria, we generated a list of 10 top candidate genes (Table 2). Of the probes examined, we observed the expression of CARTPT (Cocaine- And Amphetamine-Regulated Transcript Protein), a neuropeptide implicated in feeding, reward, and stress (Carpenter et al., 2020; Funayama et al., 2022; Kristensen et al., 1998; Lee et al., 2022), to be the most lineage segregated. We found high expression of CARTPT in the MeA (Figure 5a) and in a pattern strikingly resembling

the distribution of *Dbx1*-lineage neurons (Figure 5b-e), and complementary to the distribution of *Foxp2*+ neurons (Figure 5f-h). Dual immunofluorescence revealed that the majority of CARTPT+ cell bodies and projections were embedded within regions of *Dbx1*-lineage neurons (Figure 5e). In contrast, CARTPT+ cell bodies and projections did not co-localize with *Foxp2*+ neurons (Figure 5h). We next assessed the expression of the other nine candidates by multiplexed RNAscope™ in situ hybridization in the MeA (Figure 6). Of these, we confirmed the expression of all candidates except *Npy1r*. Of the markers expressed in the MeA, most were expressed only in a small subset of either *Dbx1*-lineage or *Foxp2*+ neurons. Of these markers, we found three *Tac2*, *Ucn3*, and *Npy* were expressed significantly more in neurons of one lineage versus the other. We found both *Tac2* and *Npy* mRNA were modestly but significantly enriched in *Dbx1*-lineage neurons relative to *Foxp2* mRNA+ neurons (Figure 6a-a",c-c"). In contrast, we found *Ucn3* mRNA, which encodes the Urocortin 3 peptide, enriched in *Foxp2* mRNA+ neurons in the MeA (Figure 6b-b").

3.4 | Sex differences in inhibitory and excitatory input to MeA *Foxp2*- and *Dbx1*-lineages

In addition to molecular differences described above and by Lischinsky et al. (2017) between MeA *Foxp2*- and *Dbx1*-lineage neurons, our previous studies revealed lineage differences in intrinsic biophysical properties (Matos et al., 2020). Prior studies from others revealed male/female differences in total inputs to the MeA, with males displaying more excitatory input (Billing et al., 2020; Cooke & Woolley, 2005). However, the MeA neuronal subtype targets of these inputs remain unknown. Therefore, we next conducted patch-clamp electrophysiology and measured spontaneous postsynaptic currents (sPSCs), a measure of synaptic activity, in EYFP+ MeA neurons in *Foxp2^{cre};RYFP* and *Dbx1^{cre};RYFP* mice of both sexes (Figure 7a,b). Gap-free recordings in ACSF at a holding potential of -60 mV largely measured spontaneous AMPA/kainate receptor-mediated currents (sEPSCs; Figure 7c). We found a significantly higher frequency of total sEPSCs (Figure 7d) in male *Dbx1*-lineage neurons compared to male *Foxp2*-lineage neurons. We additionally observed that *Foxp2*-lineage neurons in females displayed a significantly higher event frequency than those in males, while the opposite was true for *Dbx1*-lineage neurons (Figure 7d). Further, *Foxp2*-lineage neurons receive lower excitatory input than *Dbx1*-lineage neurons in males (Figure 7d), a finding consistent with our previous observations (Lischinsky et al., 2017).

As we observed sex differences in sPSC recordings within MeA *Foxp2*-lineage neurons (Figure 7d), we next wanted to assess whether there were corresponding differences in the expression of either excitatory or inhibitory synaptic markers on MeA *Foxp2*-lineage neurons. To accomplish this, we assessed the expression of the excitatory pre- and postsynaptic markers, PSD95 and VGLUT2, and the inhibitory pre- and postsynaptic markers, Gephyrin and VGAT, in *Foxp2^{cre};RYFP* mice by immunohistochemistry (Figure 8). We quantified both the proportion of *Foxp2*-lineage (EYFP+) neurons receiving excitatory

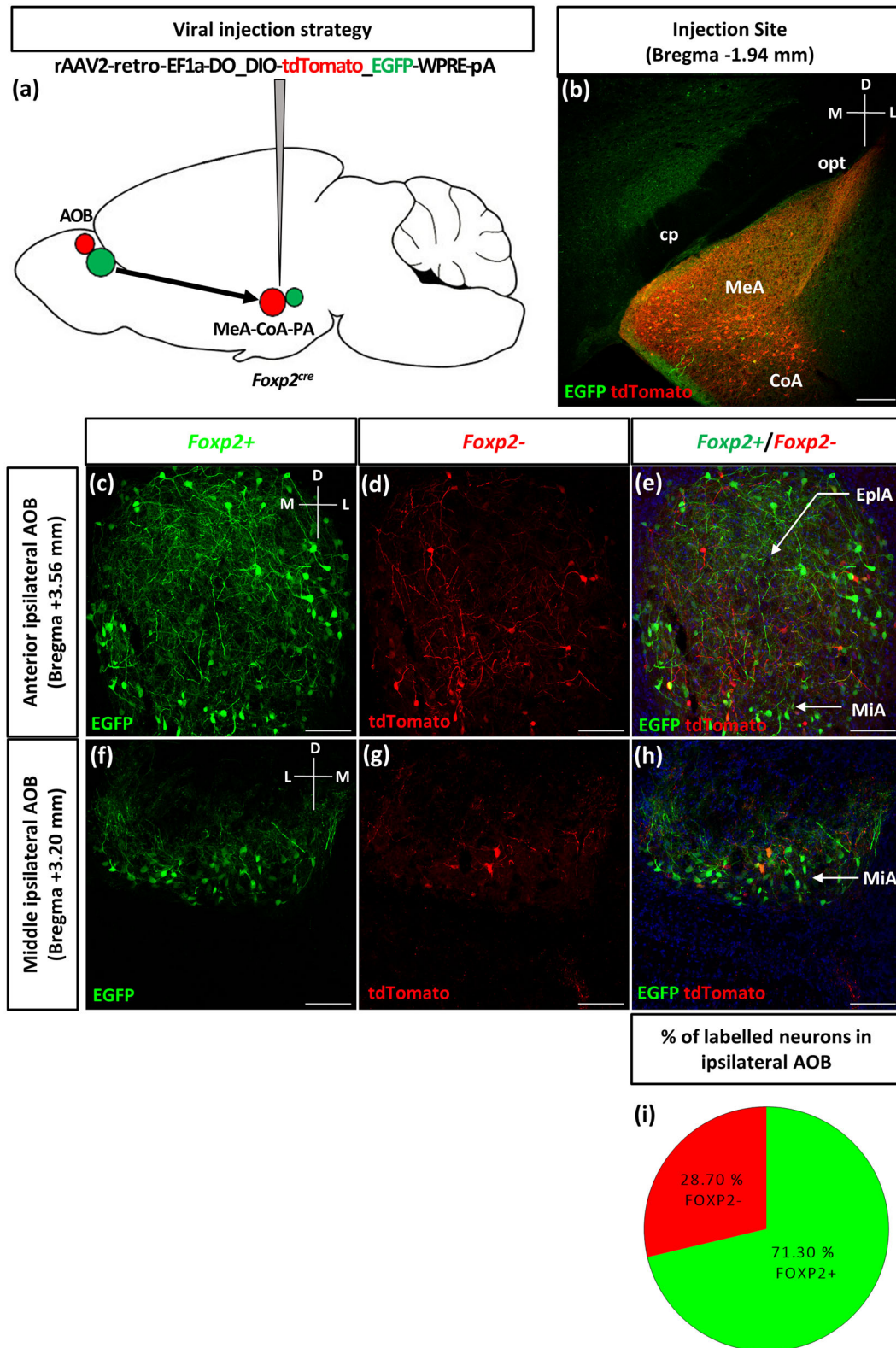


FIGURE 4 Retrograde tracing of accessory olfactory bulb (AOB) inputs to medial amygdala (MeA) neurons. (a) Schematic diagram illustrating the injection strategy of dual-switch retrograde AAV transduction in the medial, cortical, and posterior nuclei of the amygdala (MeA-CoA-PA) in *Foxp2*^{cre} mice. (b) Representative immunofluorescence image of a coronal section at the injection site shows strong viral expression in the posterior MeA (Bregma -1.94 mm). (c-e) Immunofluorescence images of the ipsilateral anterior AOB (coronal section, Bregma +3.56 mm) show *Foxp2*⁺ (recombined EGFP+, green, c) and *Foxp2*⁻ (non-recombined tdTomato+, red, d) neurons. Merged image (e) reveals very minimal overlap of EGFP and tdTomato. (f-h) Immunofluorescence images of the ipsilateral middle AOB (coronal section, Bregma +3.20 mm) show similar recombination in

(Continues)

FIGURE 4 (Continued)

the middle AOB. Crosses indicate section orientation (D, dorsal; M, medial; L, lateral). (i) Pie chart showing quantification of the percentage of *Foxp2*+ (green) and *Foxp2*- (red) ipsilateral AOB output neurons projecting to the MeA-CoA-PA. CoA, cortical amygdala; cp, cerebral peduncle; EplA, external plexiform layer of the AOB; MiA, mitral cell layer of the AOB; opt, optic tract. Scale bar equals 200 μ m in panel (b) and 100 μ m in all other panels. $n = 7$ mice (4 females and 3 males, 10–17 sections/mouse).

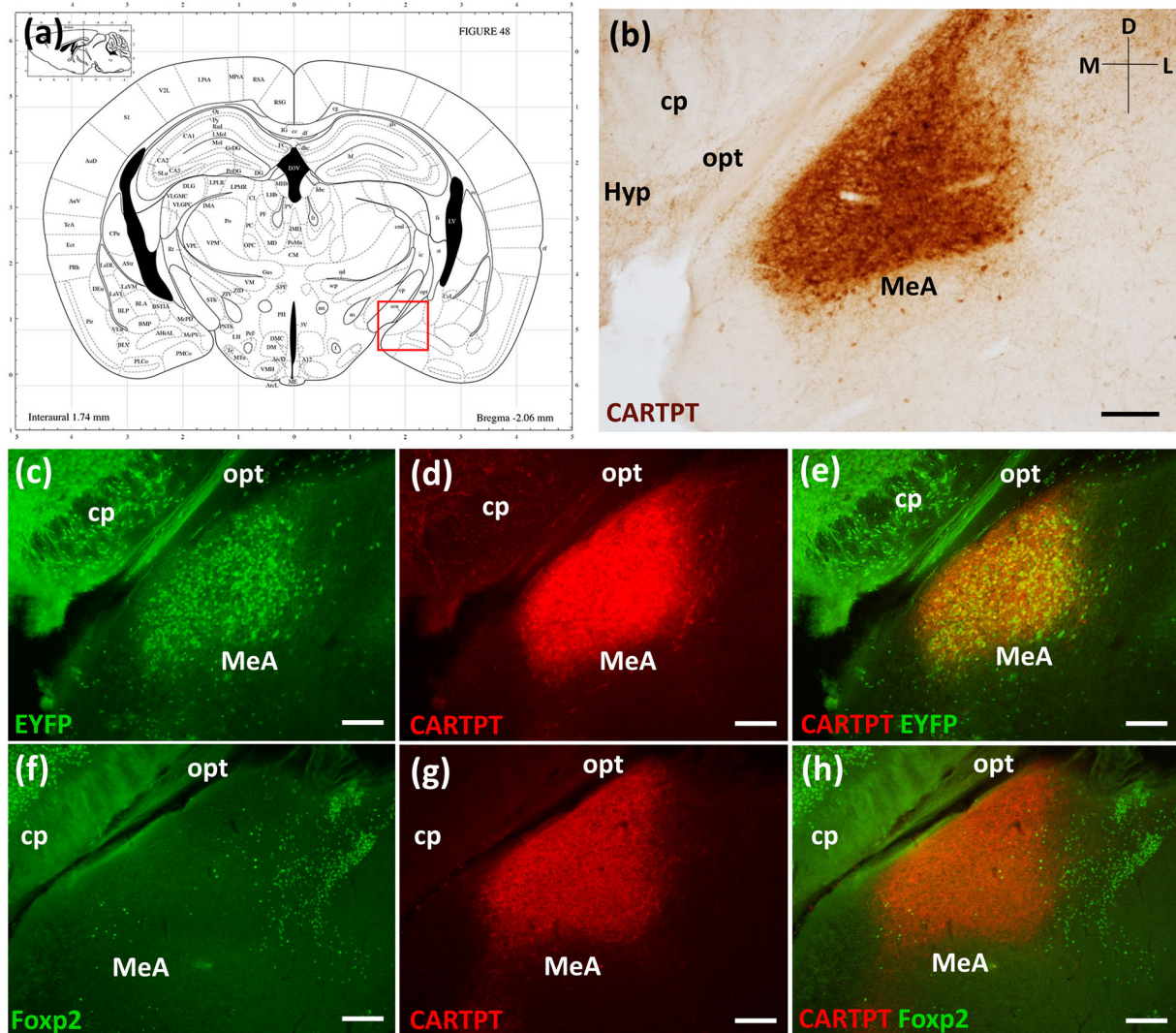


FIGURE 5 Distribution of *Dbx1*-lineage and *Foxp2*+ neurons in the medial amygdala (MeA) in relation to CARTPT expression. (a) Image from Franklin and Paxinos (2008) showing the posterior MeA (red box) in coronal view at the same antero-posterior level as the sections shown in panels (b–h). (b) Brightfield immunohistochemistry image showing CARTPT expression localized in the posterodorsal MeA. (c–e) Immunofluorescence image showing *Dbx1*-lineage neurons (EYFP+, green, c) and CARTPT+ cell bodies and fibers (red, d) in the MeA of a *Dbx1^{Cre};RYFP* mouse. CARTPT expression matches the distribution of *Dbx1*-lineage neurons that are observed embedded within a zone of CARTPT immunoreactivity (e). (f–h) Complementary distribution of *Foxp2*+ neurons (green, f) to the expression pattern of CARTPT (red, g), with *Foxp2*+ neurons predominantly observed outside the zone of CARTPT expression (h). Cross in panel (b) indicates section orientation (D, dorsal; M, medial; L, lateral), same followed in panels (c–h). cp, cerebral peduncle; Hyp, hypothalamus; opt, optic tract. All scale bars equal 200 μ m.

and inhibitory inputs as well as the number of colocalized pre- and postsynaptic excitatory or inhibitory puncta on EYFP+ neurons. We established a threshold of five or more puncta on an EYFP+ neuron as positive for the corresponding marker. We found that a subset of *Foxp2*-lineage neurons in both males and females received putative

direct excitatory (Figure 8a–e) or inhibitory (Figure 8g–k) input. However, we found no differences in the proportion of neurons receiving excitatory (Figure 8f) or inhibitory (Figure 8l) input in males compared to females, nor in the number of puncta on each EYFP+ neuron (data not shown).

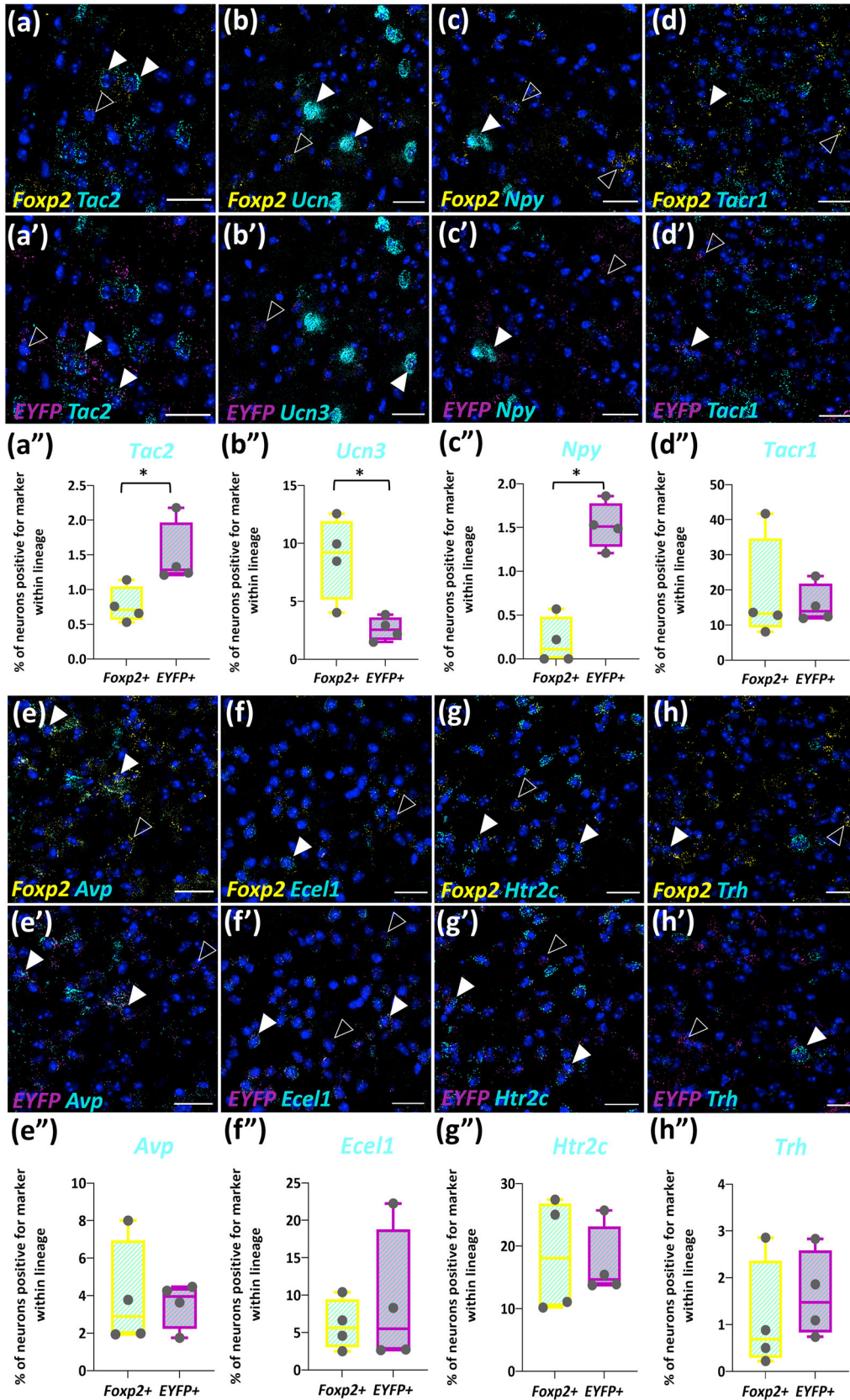


FIGURE 6 Fluorescent in situ hybridization for neuropeptides and receptors in *Foxp2*+ and *Dbx1*-lineage neurons in the medial amygdala (MeA). (a–a'') Expression and quantification of *Tac2* mRNA (cyan)-expressing neurons within *Foxp2* mRNA+ (yellow, a) and *Dbx1*-lineage (*EYFP* mRNA+, magenta, a') neurons, as shown in coronal sections from the posterodorsal MeA. (a'') Box-and-whisker plots show percentage of co-expression of *Tac2* mRNA within each population. (b–h'') Expression and quantification of the following other mRNAs: *Ucn3* (b–b''), *Npy* (c–c''),

(Continues)

FIGURE 6 (Continued)

Tacr1 (d–d’), *Avp* (e–e’), *Ecel1* (f–f’), *Htr2c* (g–g’), and *Trh* (h–h’). Solid white arrowheads indicate neurons double positive for *Foxp2* or *EYFP* mRNA and the candidate gene mRNA; empty white triangles indicate neurons positive for *Foxp2* or *EYFP* mRNA but not the candidate gene mRNA. Scale bars equal 25 μ m for all images. *False discovery rate (FDR)-adjusted *p* value <.05 after multiple Mann–Whitney *U*-tests. All other comparisons not significant (FDR-adjusted *p* > .05). *n* = 4 male mice (2–4 sections/mouse, bilateral counts).

TABLE 2 List of neuropeptide and receptor candidate genes expressed in the MeA and previously implicated in social or other behaviors.

Gene symbol	Gene name	Behaviors implicated in	References
<i>Tac2</i>	Tachykinin 2	Aggression, freezing (fear)	Asahina et al., 2014; Zelikowsky et al., 2018
<i>Ucn3</i>	Urocortin 3	Aggression, social novelty preference	Autry et al., 2021; Shemesh et al., 2016
<i>Npy</i>	Neuropeptide Y	Aggression, social interaction/social anxiety, maternal behavior	Karl et al., 2004; Muroi & Ishii, 2015; Sajdyk et al., 1999, 2002
<i>Tacr1</i> (<i>Nk1r</i>)	Tachykinin receptor 1 (Neurokinin 1 receptor)	Aggression, mating	Berger et al., 2012; Halasz et al., 2009
<i>Avp</i>	Arginine vasopressin	Aggression, social interaction, pair bonding	Donaldson et al., 2010; Gutzler et al., 2010; Koolhaas et al., 1990; Terranova et al., 2017; Whylings et al., 2020
<i>Ecel1</i>	Endothelin converting enzyme-like 1	Aggression, social behavior	Delprato et al., 2018; Xu et al., 2012
<i>Htr2c</i>	Serotonin (5-HT) receptor 2C	Social interaction/social anxiety, social novelty, freezing (fear), aggression	Martin et al., 2012; Séjourné et al., 2015
<i>Trh</i>	Thyrotropin releasing hormone	Social interaction, aggression	Crowley & Hyding, 1976; Kwon et al., 2021; Pucikowski et al., 1988
<i>Npy1r</i>	Neuropeptide Y receptor Y1	Aggression, social interaction/social anxiety	Padilla et al., 2016; Sajdyk et al., 1999
<i>Cartpt</i>	Cocaine- and amphetamine- regulated transcript protein prepropeptide	Feeding, cocaine/reward-seeking, stress resiliency, social dominance and aggression	Carpenter et al., 2020; Funayama et al., 2022; Kristensen et al., 1998; Lee et al., 2022

4 | DISCUSSION

4.1 | Summary of findings

Using a combination of gene expression analyses and viral circuit mapping approaches, we revealed the molecular diversity and patterns of connectivity of neurons within core structures of the AOS, VNO, AOB, and MeA. We find that two transcription factor-expressing populations, *Foxp2*+ neurons and neurons derived from the *Dbx1* lineage, define molecularly distinct neuronal populations across brain nuclei that comprise the AOS. We further find that *Foxp2*+ neurons in the AOB comprise the overwhelming majority of outputs to the MeA. Interestingly, we further find sex differences in the electrophysiologically recorded frequency of inputs to MeA neurons. Our findings suggest that subpopulations of neurons identified by ongoing or prior expression of select transcription factors may define distinct subcircuits within the AOS and uncover a sexual dimorphism in their input connectivity.

4.2 | Lineage diversity across an interconnected circuit

The AOS is dedicated to processing innate behaviors such as mating, aggression, and predator avoidance. These behaviors are considered “hardwired,” meaning that they manifest without prior behavioral training. Although shaped by hormonal influences, the patterns of wiring of these circuits are likely in large part predetermined by developmental genetic programs. However, these genetic programs remain unknown. Our previous studies and the studies of others linking MeA embryonic development to neuronal diversity (Aerts & Seuntjens, 2021; Carney et al., 2010; García-Moreno et al., 2010; Lischinsky et al., 2017) revealed that embryonic expression of the transcription factors *Otp*, *Foxp2*, and *Dbx1* defines separate populations of neural progenitors that later give rise to non-overlapping populations of either excitatory (*Otp*) or inhibitory (*Foxp2*, *Dbx1*) MeA output neurons. Across the developing nervous system, expression of discrete subclasses of transcription factors in neural progenitors directs the emergence of

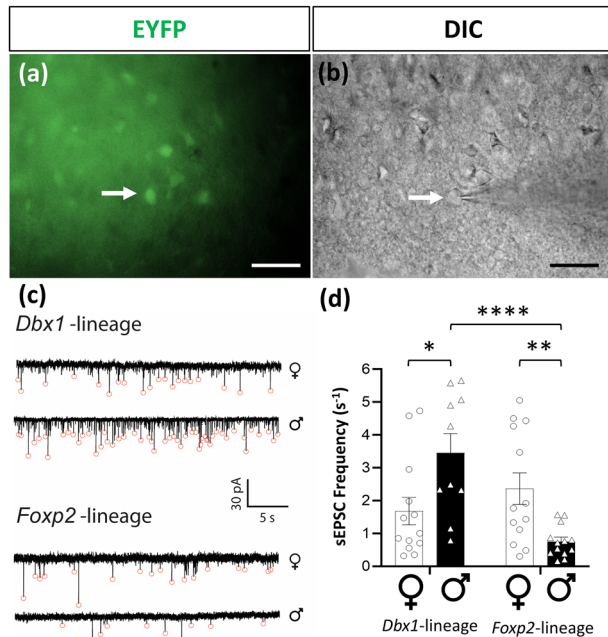


FIGURE 7 Sex and lineage differences in the frequency of spontaneous excitatory postsynaptic currents (sEPSCs). (a) Representative epifluorescence and (b) Differential Interference Contrast images show a representative recombined EYFP+ neuron (white arrows) in the posterior MeA targeted for ex vivo patch electrophysiology. (c) Representative current traces in whole-cell voltage clamp mode (-60 mV holding potential) from *Dbx1*-lineage (top) or *Foxp2*-lineage (bottom) neurons with traces from females and males shown separately. Orange circles indicate counted sEPSC events. (d) Quantification of frequency (events per second plotted as mean \pm SEM) of sEPSCs in *Dbx1*-lineage (left) or *Foxp2*-lineage (right) neurons in ACSF, from female (circles, white bar) or male (triangles, black bar) mice. * $p < .05$; ** $p < .01$; **** $p < .0001$; other pairwise comparisons not significant, $\alpha = .05$ (two-way ANOVA and Sidak's post hoc test). $n = 10$ – 13 neurons from 5–7 mice/group. Scale bars equal $50 \mu\text{m}$ in panels (a) and (b).

later neuronal subtype identity (Aydin et al., 2019; Heavner et al., 2020; Hörmann et al., 2020; Sagner et al., 2021). The early endowment of MeA neuronal diversity as defined by transcription factor expression (*Otp*, *Foxp2*, *Dbx1*) suggests a potential molecular code for how the MeA is assembled. Here, our gene expression analysis revealed that this molecular coding may be at least partially conserved in the VNO and AOB, which lie one and two nodes upstream of the MeA, respectively. We found that in addition to the MeA, *Dbx1*-lineage neurons mark subsets of sensory neurons in the VNO and output neurons in the AOB. In the VNO, *Dbx1*-lineage neurons comprise $\sim 7\%$ of the entire sensory neuron population across both apical and basal layers. A recent study revealed that *Dbx1* is expressed as early as Embryonic day 12.5 in the developing VNO (Causseret et al., 2023). Thus, similar to other regions of the nervous system, *Dbx1* also marks early developing progenitors in the VNO. As the VNO is the first site of sensory processing in the AOS, it is interesting to speculate that *Dbx1*-lineage sensory neurons may express specific subclasses of olfactory receptors implicated in select innate behaviors. If this is the case, it also raises

the intriguing possibility that neurons of the same transcription factor identity/lineage (in this case *Dbx1*) directly connect with each other to form a transcription factor-labeled line for the processing of select olfactory cues. However, the case for a potential labeled-line circuit is not as strong for neurons marked by *Foxp2*. In contrast to the *Dbx1* lineage, *Foxp2* marks a much larger population of AOB neurons, comprising more than two thirds of the output neurons projecting directly to the MeA. The lower number of *Dbx1*-lineage neurons in the AOB precluded our ability to trace *Dbx1*-lineage AOB projections to their final destinations using anterograde viral tracing. However, it would be reasonable to assume that AOB *Dbx1*-lineage neurons in part comprise the MeA-projecting *Foxp2*-negative population. Regardless, combined with our previous findings (Lischinsky et al., 2017), our current findings reveal that within and outside the MeA, expression of the same transcription factors defines regions of a known accessory olfactory circuit.

4.3 | MeA neuropeptide expression

Our previous studies revealed that *Foxp2*- and *Dbx1*-lineage neurons in the MeA express cohorts of sex hormone-related proteins and ion channels in a lineage-specific manner. Aromatase and ER- α , and the action potential regulating ion channels *Kir5.1*, *Kir6.1*, *KChip4.1*, *Cav1.2*, and *Kv7.1*, are all expressed in a greater proportion of *Dbx1*-lineage neurons, whereas the ion channel *Kir2.1* is expressed in a greater proportion in the *Foxp2* lineage (Lischinsky et al., 2017; Matos et al., 2020). Here, we extended this prior knowledge by assessing expression of neuropeptides known to have a function in MeA-regulated behaviors such as feeding, aggression, and mating. We show that expression of *CARTPT*, *Tac2*, and *Npy* is enriched in the *Dbx1* lineage, while *Ucn3* is expressed in more *Foxp2* mRNA+ neurons than *Dbx1*-lineage neurons. Of these, the most interesting pattern was that of *CARTPT*, whose expression pattern strikingly mimics the distribution of *Dbx1*-lineage neurons. As the *CARTPT* antibody marks both cell bodies and *CARTPT*+ fibers, it was difficult to discern if *Dbx1*-lineage neurons are producing *CARTPT* or receiving dense *CARTPT*+ input. Regardless, the strong expression overlap implicates MeA *Dbx1*-lineage neurons in aspects of feeding, homeostasis, and/or reward. In addition, our multiplexed RNAscope™ in situ hybridization analyses revealed a higher expression of *Tac2* and *Npy* in *Dbx1*-lineage neurons, implicating MeA *Dbx1*-lineage neurons in aggression, social novelty, or sexual arousal. *Tac2* encodes a neuropeptide, tachykinin isoform 2, that promotes aggressive behavior in fruit flies and mice (Asahina et al., 2014; Zelikowsky et al., 2018). *Npy* encodes Neuropeptide Y that, in rodents, modulates aggression through Y1 receptors in the MeA (Karl et al., 2004), is implicated in reduced social anxiety (Sajdyk et al., 1999, 2002), and regulates maternal behavior, a critical sex-specific social behavior (Muroi & Ishii, 2015). In contrast, of the 10 neuropeptides explored, we found only *Ucn3* to be enriched in the *Foxp2* mRNA+ population. Urocortin 3 has been shown to promote preference for social novelty through its action in the MeA (Shemesh et al., 2016), infant-directed aggression through its function in the perifornical area of the

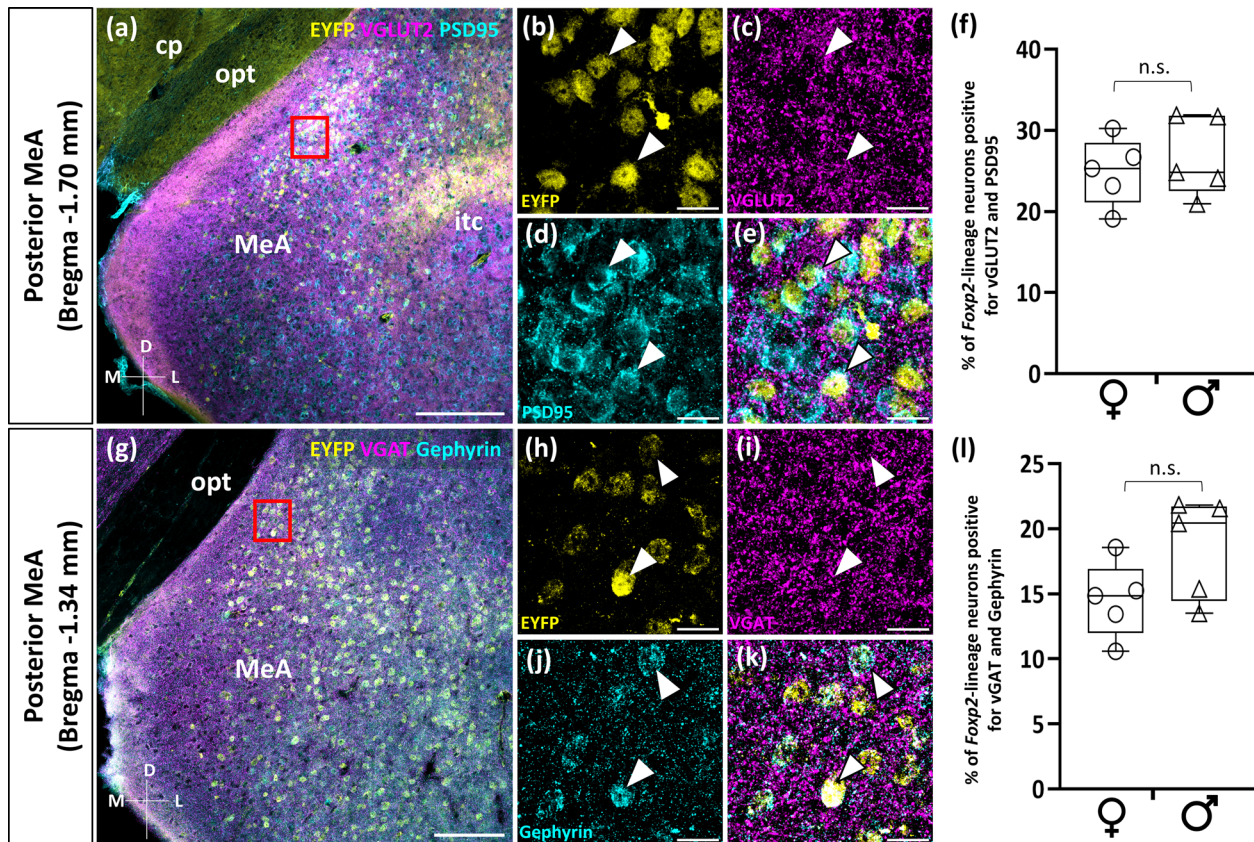


FIGURE 8 MeA *Foxp2*-lineage neurons receive excitatory and inhibitory inputs, with no sex differences. (a) Posterior MeA *Foxp2*-lineage neurons (EYFP+, yellow), identified by immunofluorescence in coronal sections from *Foxp2^{cre};RYFP* mice and co-immunostained for the excitatory pre- and postsynaptic markers, VGLUT2 (magenta) and PSD95 (cyan), respectively. (b–e) Higher magnification images of boxed region in panel (a), with EYFP (b, yellow), VGLUT2 (c, magenta), and PSD95 (d, cyan) channels shown separately. Merged image (e) shows *Foxp2*-lineage neurons expressing PSD95 and surrounded by VGLUT2 puncta (solid white arrowheads in panels [b–e]), indicating putative excitatory synapses. (f) Box-and-whisker plots quantifying *Foxp2*-lineage neurons positive for both VGLUT2 and PSD95, plotted as a percentage of total *Foxp2*-lineage (EYFP+) neurons in the posterior MeA, comparing females versus males. (g) Posterior MeA *Foxp2*-lineage neurons (EYFP+, yellow), co-immunostained for the inhibitory pre- and postsynaptic markers, VGAT (magenta) and Gephyrin (cyan), respectively. (h–k) Higher magnification images of boxed region in panel (g), with EYFP (h, yellow), VGAT (i, magenta), and Gephyrin (j, cyan) channels shown separately. Merged image (k) shows *Foxp2*-lineage neurons expressing Gephyrin and surrounded by VGAT puncta (solid white arrowheads in panels [h–k]), indicating putative inhibitory synapses. (l) Box-and-whisker plots quantifying *Foxp2*-lineage neurons positive for both VGAT and Gephyrin, plotted as a percentage of total *Foxp2*-lineage (EYFP+) neurons in the posterior MeA, comparing females versus males. Crosses in panels (a) and (g) indicate section orientation (D, dorsal; M, medial; L, lateral). cp, cerebral peduncle; itc, intercalated nucleus of the amygdala; MeA, medial amygdala; opt, optic tract. Scale bars in panels (a) and (g) equal 250 μ m. In all other panels, scale bars equal 20 μ m. n.s. indicates not significant ($p > .05$, Mann–Whitney *U* test). $n = 5$ mice per sex (3 sections/mouse, bilateral counts).

hypothalamus (Autry et al., 2021), and feeding (Stengel & Taché, 2014). This suggests a role for *Foxp2*+ neurons in these behaviors and is consistent with the role of the *Foxp2* gene and *Foxp2*+ neurons in aggression (Herrero et al., 2021; Lischinsky et al., 2017, 2023). Aside from CARTPT, it is important to note that although lineage restricted, *Tac2*, *Npy*, and *Ucn3* are only expressed in a small subset of neurons. This, however, does not preclude a putative important lineage-specific role in behavior for the following reasons: First, our expression analysis was conducted using tissue from home-cage animals. As levels of neuropeptide expression are typically state dependent, it is likely we are observing only a baseline of expression, which may change over time. Second, our prior studies of cFos activation patterns in the MeA revealed that even during behavioral tasks that elicit a strong behav-

ioral response, cFos is expressed only in a subset of neurons within each lineage (Lischinsky et al., 2017). This indicates that perhaps only a handful of neurons within a given population needs to be active to be engaged in a given behavior. Third, these (and other) neuropeptides may act in concert in overlapping or different populations to modulate behavior. While these lineage-specific expression patterns of neuropeptides importantly extend our knowledge of molecular diversity of MeA neurons, it remains to be determined how different behaviors are regulated by each lineage, as there are many mechanisms beyond neuropeptide expression that influence behavior. These include, for examples, patterns and types of input/output connectivity and intrinsic neuronal excitability and other biophysical parameters. Future transcriptomic analysis of *Foxp2*- and *Dbx1*-lineage neurons will be highly

informative in providing a fuller picture of the molecular diversity of these populations.

4.4 | Sex differences in connectivity

The MeA has been long recognized as a highly sexually dimorphic brain region, with known differences in structural properties such as cell morphology, dendritic complexity, and cell size (Cooke & Woolley, 2005; Cooke et al., 2007; Hines et al., 1992). Our prior patch-clamp electrophysiology studies further revealed sex differences in intrinsic biophysical properties, including action potential firing dynamics in both *Foxp2* and *Dbx1* lineages (Matos et al., 2020). Moreover, recent gene expression and single-cell RNA-seq transcriptomic studies revealed sex differences at the molecular level in the MeA (Chen et al., 2019). Interestingly, the sex differences in gene expression in the MeA were most prominent in inhibitory GABAergic neurons as opposed to the excitatory glutamatergic population.

While our previous work revealed that *Dbx1*-lineage neurons receive greater excitatory input than *Foxp2*-lineage neurons (Lischinsky et al., 2017), we did not explore whether there were sex differences in inputs to these two GABAergic output populations. To examine this, here we took both an electrophysiological approach by measuring the frequency of spontaneous inputs and an immunohistochemical approach to assess putative synaptic connectivity using well-characterized markers of excitatory and inhibitory synapses. Via patch-clamp analyses, we uncovered sex differences in total inputs to *Foxp2*- and *Dbx1*-lineage neurons. We found that *Foxp2*-lineage neurons in females have more spontaneous inputs than in males, while the opposite is true for *Dbx1*-lineage neurons. There are several possible mechanisms that can account for these observations. First, the number of excitatory and/or inhibitory synaptic inputs may be sexually dimorphic. However, our immunohistochemical analysis of synaptic markers in *Foxp2*-lineage neurons suggests that this may not be the case. Although we cannot rule out that ultrastructural analysis of synapses at a higher resolution would uncover differences, our data suggest other mechanisms may be occurring. These include sex differences in presynaptic firing rate and/or number of presynaptic neurotransmitter release events or postsynaptic membrane excitability via differences in ion channel expression. Further clues to the underlying mechanism may be inferred from recent MeA RNA-seq studies (Chen et al., 2019), which revealed major transcriptomic sex differences in MeA GABAergic neurons in genes implicated in synaptic function and communication. Although we do not know whether these differences come from within the *Foxp2* and/or *Dbx1* lineages, our electrophysiological findings provide an entry point to link sex differences in gene expression with sex differences in synaptic input that we observe in MeA *Dbx1*- and *Foxp2*-lineage neurons.

Interestingly, prior electrophysiological studies revealed that the MeA receives more excitatory input in males than in females (Cooke & Woolley, 2005). A more recent anatomical study showed that MeA Aromatase+ neurons in males receive more inputs from the AOB than in females (Dwyer et al., 2022). While in potential contrast to our find-

ings of greater synaptic input to *Foxp2*-lineage neurons in females, it is likely that the male/female pattern of inputs to the MeA varies from population to population, with some neuronal subtypes receiving more (or stronger) inputs in males and others in females. In addition to the *Foxp2*- and *Dbx1*-lineage neurons, the MeA is populated by a vast array of interneurons, excitatory (*Otp*+) output neurons (Chen et al., 2019; Lischinsky et al., 2017) and likely other inhibitory and/or excitatory output neurons not of the *Foxp2*, *Dbx1*, or *Otp* lineages. The MeA receives strong input from not only the AOB, but also from the posterior amygdala, cortical amygdala, and BNST, as well as lesser input from other brain regions (Cádiz-Moretti et al., 2014; Lischinsky et al., 2023). Thus, there are likely sex differences based not only on which MeA population is innervated, but also on source of input. Regardless of the underlying mechanism, our study introduces an additional layer of refinement in the analysis of physiological inputs to the MeA via developmental transcription factor-defined subpopulations.

Although we found robust differences across sex in synaptic input as uncovered by patch-clamp electrophysiology, it is important to note that in our analysis we did not segregate females based on estrus cycle. Prior work in the MeA (Dalpian et al., 2019) and the hypothalamus (Dias et al., 2021; Yin et al., 2022) revealed estrus state-dependent changes in the strength of neuronal connectivity. Moreover, hormones greatly shape brain development at several levels. In addition to the estrus state-dependent short-term hormonal cycling that transiently affects circuitry, developmental hormonal surges also have an impact on how these circuits are initially wired together (Simerly, 2003). As the MeA plays a central role in regulating sex-specific innate behaviors such as aggression and mating, there may also be non-hormonally driven genetic programs that are involved in the establishment of male and female differences in wiring patterns during early postnatal development. Exploration of both these intrinsic and extrinsic influences on induction and maintenance of sexually dimorphic patterns of MeA connectivity and ultimately behavior will continue to be an interesting area of investigation.

AUTHOR CONTRIBUTIONS

Nandkishore Prakash, Heidi Y. Matos, and Sonia Sebaoui were involved in study design, implementation strategies, data generation, data analysis, and data interpretation and oversaw trainees and staff in this project. Nandkishore Prakash with Joshua G. Corbin prepared figures and wrote and edited the manuscript. Tuyen Tran under the direction of Katie Sokolowski generated the data in Figure 1. Julieta Lischinsky, Tsutomu Hirata, and Nandkishore Prakash generated the data in Figure 2. Nandkishore Prakash analyzed the data in Figure 2. Luke Tsai under the direction of Heidi Y. Matos generated the data in Figure 4. Shigeyuki Esumi and Julieta Lischinsky generated the data in Figure 5. Nandkishore Prakash generated and analyzed the data in Figure 6, with technical assistance from Nya Campbell in quantification and figure preparation. Heidi Y. Matos generated the data in Figure 7. Heidi Y. Matos, Hassan Hosseini, and Kevin S. Jones analyzed the data in Figure 7. Sonia Sebaoui generated and analyzed the data in Figures 3 and 8. Nandkishore Prakash performed all statistical analysis. Adejimi Aromolaran, Isabella Atrachji, Meredith Goodrich, David

Hernandez-Pineda, and Wendolin Martinez assisted in technical aspects of data generation and analysis. Maria Jesus Herrero, Shisui Torii, Satoshi Yamashita, Yuka Imamura Kawasawa, and Nandkishore Prakash generated probe lists for Table 2. Kazue Hashimoto-Torii oversaw and worked with Shisui Torii, Satoshi Yamashita, and Yuka Imamura Kawasawa. Kevin S. Jones mentored Hassan Hosseini, co-mentored Heidi Y. Matos with Joshua G. Corbin, and provided critical feedback on electrophysiology data. Joshua G. Corbin oversaw all aspects of the project from conception to execution.

ACKNOWLEDGMENTS

We kindly acknowledge intellectual input from members of the Corbin laboratory, present and past, and constructive feedback from the Haydar laboratory in the Center for Neuroscience Research at Children's National Hospital. We also thank Dr. Alla Y. Karapova at Janelia Farms, VA, for providing technical advice on the Retro-AAV2 virus.

CONFLICT OF INTEREST STATEMENT

The authors declare no conflicts of interest.

DATA AVAILABILITY STATEMENT

The data that support the findings of this study are available from the corresponding authors upon reasonable request.

ORCID

Nandkishore Prakash  <https://orcid.org/0000-0003-1619-3057>

Heidi Y. Matos  <https://orcid.org/0000-0002-5486-0773>

Sonia Sebaoui  <https://orcid.org/0000-0002-8920-6202>

Luke Tsai  <https://orcid.org/0000-0002-8787-5277>

Maria Jesus Herrero  <https://orcid.org/0000-0001-7432-3468>

Julieta Lischinsky  <https://orcid.org/0000-0003-1664-6642>

Hassan Hosseini  <https://orcid.org/0000-0002-2702-6994>

Yuka Imamura Kawasawa  <https://orcid.org/0000-0002-8638-6738>

Kevin S. Jones  <https://orcid.org/0000-0001-5281-1591>

Joshua G. Corbin  <https://orcid.org/0000-0003-0122-4324>

PEER REVIEW

The peer review history for this article is available at <https://publons.com/publon/10.1002/cne.25545>.

REFERENCES

- Adam, Y., Livneh, Y., Miyamichi, K., Groysman, M., Luo, L., & Mizrahi, A. (2014). Functional transformations of odor inputs in the mouse olfactory bulb. *Frontiers in Neural Circuits*, 8, 129. <https://doi.org/10.3389/fncir.2014.00129>
- Aerts, T., & Seuntjens, E. (2021). Novel perspectives on the development of the amygdala in rodents. *Frontiers in Neuroanatomy*, 15, 786679. <https://doi.org/10.3389/FNANA.2021.786679>
- Asahina, K., Watanabe, K., Duistermars, B. J., Hoopfer, E., González, C. R., Eyjólfsson, E. A., Perona, P., & Anderson, D. J. (2014). Tachykinin-expressing neurons control male-specific aggressive arousal in *Drosophila*. *Cell*, 156(1–2), 221–235. <https://doi.org/10.1016/J.CELL.2013.11.045>
- Autry, A. E., Wu, Z., Kapoor, V., Kohl, J., Bambah-Mukku, D., Rubinstein, N. D., Marin-Rodriguez, B., Carta, I., Sedwick, V., Tang, M., & Dulac, C. (2021). Urocortin-3 neurons in the mouse perifornical area promote infant-directed neglect and aggression. *eLife*, 10, e64680. <https://doi.org/10.7554/ELIFE.64680>
- Aydin, B., Kakumanu, A., Rossillo, M., Moreno-Estellés, M., Garipler, G., Ringstad, N., Flames, N., Mahony, S., & Mazzoni, E. O. (2019). Proneural factors *Ascl1* and *Neurog2* contribute to neuronal subtype identities by establishing distinct chromatin landscapes. *Nature Neuroscience*, 22(6), 897–908. <https://doi.org/10.1038/S41593-019-0399-Y>
- Batista-Brito, R., MacHold, R., Klein, C., & Fishell, G. (2008). Gene expression in cortical interneuron precursors is prescient of their mature function. *Cerebral Cortex*, 18(10), 2306–2317. <https://doi.org/10.1093/CERCOR/BHM258>
- Beier, C., Zhang, Z., Yurgel, M., & Hattar, S. (2021). The projections of ipRGCs and conventional RGCs to retinorecipient brain nuclei. *The Journal of Comparative Neurology*, 529(8), 1863–1875. <https://doi.org/10.1002/cne.25061>
- Ben-Shaul, Y., Katz, L. C., Mooney, R., & Dulac, C. (2010). In vivo vomeronasal stimulation reveals sensory encoding of conspecific and allospecific cues by the mouse accessory olfactory bulb. *Proceedings of the National Academy of Sciences of the United States of America*, 107(11), 5172–5177. <https://doi.org/10.1073/PNAS.0915147107>
- Bergan, J. F., Ben-Shaul, Y., & Dulac, C. (2014). Sex-specific processing of social cues in the medial amygdala. *eLife*, 3, e02743. <https://doi.org/10.7554/eLife.02743>
- Berger, A., Tran, A. H., Dida, J., Minkin, S., Gerard, N. P., Yeomans, J., & Paige, C. J. (2012). Diminished pheromone-induced sexual behavior in neurokinin-1 receptor deficient (*TACR1(-/-)*) mice. *Genes, Brain, and Behavior*, 11(5), 568–576. <https://doi.org/10.1111/J.1601-183X.2012.00787.X>
- Bian, X. (2013). Physiological and morphological characterization of GABAergic neurons in the medial amygdala. *Brain Research*, 1509, 8–19. <https://doi.org/10.1016/J.BRAINRES.2013.03.012>
- Bian, X., Yanagawa, Y., Chen, W. R., & Luo, M. (2008). Cortical-like functional organization of the pheromone-processing circuits in the medial amygdala. *Journal of Neurophysiology*, 99(1), 77–86. <https://doi.org/10.1152/JN.00902.2007>
- Bielle, F., Griveau, A., Narboux-Nême, N., Vigneau, S., Sigrist, M., Arber, S., Wassef, M., & Pierani, A. (2005). Multiple origins of Cajal-Retzius cells at the borders of the developing pallidum. *Nature Neuroscience*, 8(8), 1002–1012. <https://doi.org/10.1038/nn1511>
- Billing, A., Correia, M. H., Kelly, D. A., Li, G. L., & Bergan, J. F. (2020). Synaptic connections of aromatase circuits in the medial amygdala are sex specific. *eNeuro*, 7(3), Article ENEURO.0489-19.2020. <https://doi.org/10.1523/ENEURO.0489-19.2020>
- Buck, L., & Axel, R. (1991). A novel multigene family may encode odorant receptors: A molecular basis for odor recognition. *Cell*, 65(1), 175–187. [https://doi.org/10.1016/0092-8674\(91\)90418-X](https://doi.org/10.1016/0092-8674(91)90418-X)
- Burton, S. D., Brown, A., Eiting, T. P., Youngstrom, I. A., Rust, T. C., Schmuker, M., & Wachowiak, M. (2022). Mapping odorant sensitivities reveals a sparse but structured representation of olfactory chemical space by sensory input to the mouse olfactory bulb. *eLife*, 11, e80470. <https://doi.org/10.7554/ELIFE.80470>
- Cádiz-Moretti, B., Otero-García, M., Martínez-García, F., & Lanuza, E. (2014). Afferent projections to the different medial amygdala subdivisions: A retrograde tracing study in the mouse. *Brain Structure and Function*, 221(2), 1033–1065. <https://doi.org/10.1007/S00429-014-0954-Y>
- Carney, R. S. E., Mangin, J. M., Hayes, L., Mansfield, K., Sousa, V. H., Fishell, G., Machold, R. P., Ahn, S., Gallo, V., & Corbin, J. G. (2010). Sonic hedgehog expressing and responding cells generate neuronal diversity in the medial amygdala. *Neural Development*, 5, Article 14. <https://doi.org/10.1186/1749-8104-5-14>
- Carpenter, M. D., Hu, Q., Bond, A. M., Lombroso, S. I., Czarnecki, K. S., Lim, C. J., Song, H., Wimmer, M. E., Pierce, R. C., & Heller, E. A. (2020). Nr4a1 suppresses cocaine-induced behavior via epigenetic regulation of

- homeostatic target genes. *Nature Communications*, 11, Article 504. <https://doi.org/10.1038/s41467-020-14331-y>
- Causeret, F., Fayon, M., Moreau, M. X., Ne, E., Oleari, R., Parras, C., Cariboni, A., & Pierani, A. (2023). Diversity within olfactory sensory derivatives revealed by the contribution of Dbx1 lineages. *The Journal of Comparative Neurology*, 531(12), 1229–1243. <https://doi.org/10.1002/cne.25492>
- Cavaliere, R. M., Silvotti, L., Percudani, R., & Tirindelli, R. (2020). Female mouse tears contain an anti-aggression pheromone. *Scientific Reports*, 10(1), 2510. <https://doi.org/10.1038/s41598-020-59293-9>
- Chen, P. B., Hu, R. K., Wu, Y. E., Pan, L., Huang, S., Micevych, P. E., & Hong, W. (2019). Sexually dimorphic control of parenting behavior by the medial amygdala. *Cell*, 176(5), 1206.e18–1221.e18. <https://doi.org/10.1016/j.CELL.2019.01.024>
- Chen, Y. C., Kuo, H. Y., Bornschein, U., Takahashi, H., Chen, S. Y., Lu, K. M., Yang, H. Y., Chen, G. M., Lin, J. R., Lee, Y. H., Chou, Y. C., Cheng, S. J., Chien, C. T., Enard, W., Hevers, W., Pääbo, S., Graybiel, A. M., & Liu, F. C. (2016). Foxp2 controls synaptic wiring of corticostriatal circuits and vocal communication by opposing Mef2C. *Nature Neuroscience*, 19(11), 1513–1522. <https://doi.org/10.1038/NN.4380>
- Choi, G. B., Dong, H. W., Murphy, A. J., Valenzuela, D. M., Yancopoulos, G. D., Swanson, L. W., & Anderson, D. J. (2005). Lhx6 delineates a pathway mediating innate reproductive behaviors from the amygdala to the hypothalamus. *Neuron*, 46(4), 647–660. <https://doi.org/10.1016/j.neuron.2005.04.011>
- Co, M., Hickey, S. L., Kulkarni, A., Harper, M., & Konopka, G. (2020). Cortical Foxp2 supports behavioral flexibility and developmental dopamine D1 receptor expression. *Cerebral Cortex*, 30(3), 1855–1870. <https://doi.org/10.1093/CERCOR/BHZ209>
- Cooke, B. M., Stokas, M. R., & Woolley, C. S. (2007). Morphological sex differences and laterality in the prepubertal medial amygdala. *The Journal of Comparative Neurology*, 501(6), 904–915. <https://doi.org/10.1002/CNE.21281>
- Cooke, B. M., & Woolley, C. S. (2005). Sexually dimorphic synaptic organization of the medial amygdala. *Journal of Neuroscience*, 25(46), 10759–10767. <https://doi.org/10.1523/JNEUROSCI.2919-05.2005>
- Crowley, T. J., & Hyndinger, M. (1976). MIF, TRH, and simian social and motor behavior. *Pharmacology Biochemistry and Behavior*, 5(Suppl. 1), 79–87. [https://doi.org/10.1016/0091-3057\(76\)90333-6](https://doi.org/10.1016/0091-3057(76)90333-6)
- Dalpian, F., Rasia-Filho, A. A., & Calcagnotto, M. E. (2019). Sexual dimorphism, estrous cycle and laterality determine the intrinsic and synaptic properties of medial amygdala neurons in rat. *Journal of Cell Science*, 132(9), jcs227793. <https://doi.org/10.1242/JCS.227793>
- Davis, B. J., Macrides, F., Youngs, W. M., Schneider, S. P., & Rosene, D. L. (1978). Efferents and centrifugal afferents of the main and accessory olfactory bulbs in the hamster. *Brain Research Bulletin*, 3(1), 59–72. [https://doi.org/10.1016/0361-9230\(78\)90062-X](https://doi.org/10.1016/0361-9230(78)90062-X)
- Delprato, A., Bonheur, B., Algéo, M. P., Murillo, A., Dhawan, E., Lu, L., Williams, R. W., & Crusio, W. E. (2018). A quantitative trait locus on chromosome 1 modulates intermale aggression in mice. *Genes, Brain and Behavior*, 17(7), e12469. <https://doi.org/10.1111/GBB.12469>
- Del Punta, K., Leinders-Zufall, T., Rodriguez, I., Jukam, D., Wysocki, C. J., Ogawa, S., Zufall, F., & Mombaerts, P. (2002). Deficient pheromone responses in mice lacking a cluster of vomeronasal receptor genes. *Nature*, 419(6902), 70–74. <https://doi.org/10.1038/nature00955>
- Dias, I. C., Gutierrez-Castellanos, N., Ferreira, L., & Lima, S. Q. (2021). The structural and electrophysiological properties of progesterone receptor-expressing neurons vary along the anterior-posterior axis of the ventromedial hypothalamus and undergo local changes across the reproductive cycle. *eNeuro*, 8(3), Article ENEURO.0049-21.2021. <https://doi.org/10.1523/ENEURO.0049-21.2021>
- Donaldson, Z. R., Spiegel, L., & Young, L. J. (2010). Central vasopressin V1a receptor activation is independently necessary for both partner preference formation and expression in socially monogamous male prairie voles. *Behavioral Neuroscience*, 124(1), 159–163. <https://doi.org/10.1037/A0018094>
- Druart, M., Groszer, M., & Le Magueresse, C. (2020). An etiological Foxp2 mutation impairs neuronal gain in layer VI cortico-thalamic cells through increased GABAB/GIRK signaling. *The Journal of Neuroscience*, 40(44), 8543–8555. <https://doi.org/10.1523/JNEUROSCI.2615-19.2020>
- Dulac, C. (2000). Sensory coding of pheromone signals in mammals. *Current Opinion in Neurobiology*, 10(4), 511–518. [https://doi.org/10.1016/S0959-4388\(00\)00121-5](https://doi.org/10.1016/S0959-4388(00)00121-5)
- Dulac, C., & Axel, R. (1995). A novel family of genes encoding putative pheromone receptors in mammals. *Cell*, 83(2), 195–206. [https://doi.org/10.1016/0092-8674\(95\)90161-2](https://doi.org/10.1016/0092-8674(95)90161-2)
- Dulac, C., & Wagner, S. (2006). Genetic analysis of brain circuits underlying pheromone signaling. *Annual Review of Genetics*, 40, 449–467. <https://doi.org/10.1146/annurev.genet.39.073003.093937>
- Dwyer, J., Kelly, D. A., & Bergan, J. (2022). Brain-wide synaptic inputs to aromatase-expressing neurons in the medial amygdala suggest complex circuitry for modulating social behavior. *eNeuro*, 9(2), Article ENEURO.0329-21.2021. <https://doi.org/10.1523/ENEURO.0329-21.2021>
- Enard, W., Gehre, S., Hammerschmidt, K., Hölter, S. M., Blass, T., Somel, M., Brückner, M. K., Schreiweis, C., Winter, C., Sohr, R., Becker, L., Wiebe, V., Nickel, B., Giger, T., Müller, U., Groszer, M., Adler, T., Aguilar, A., Bolle, I., ... Pääbo, S. (2009). A humanized version of Foxp2 affects cortico-basal ganglia circuits in mice. *Cell*, 137(5), 961–971. <https://doi.org/10.1016/j.cell.2009.03.041>
- Farbman, A. I., & Margolis, F. L. (1980). Olfactory marker protein during ontogeny: Immunohistochemical localization. *Developmental Biology*, 74(1), 205–215. [https://doi.org/10.1016/0012-1606\(80\)90062-7](https://doi.org/10.1016/0012-1606(80)90062-7)
- Fenwick, N. M., Martin, C. L., & Llewellyn-Smith, I. J. (2006). Immunoreactivity for cocaine- and amphetamine-regulated transcript in rat sympathetic preganglionic neurons projecting to sympathetic ganglia and the adrenal medulla. *The Journal of Comparative Neurology*, 495(4), 422–433. <https://doi.org/10.1002/CNE.20870>
- Fishilevich, E., & Vosshall, L. B. (2005). Genetic and functional subdivision of the *Drosophila* antennal lobe. *Current Biology*, 15(17), 1548–1553. <https://doi.org/10.1016/j.cub.2005.07.066>
- Franklin, K., & Paxinos, G. (1997). *The mouse brain in stereotaxic coordinates: Compact first edition* (1st Ed.). Academic Press.
- Franklin, K., & Paxinos, G. (2008). *The mouse brain in stereotaxic coordinates: Compact third edition* (3rd Ed.). Academic Press.
- French, C. A., Groszer, M., Preece, C., Coupe, A. M., Rajewsky, K., & Fisher, S. E. (2007). Generation of mice with a conditional Foxp2 null allele. *Genesis*, 45(7), 440–446. <https://doi.org/10.1002/DVG.20305>
- Funayama, Y., Li, H., Ishimori, E., Kawatake-Kuno, A., Inaba, H., Yamagata, H., Seki, T., Nakagawa, S., Watanabe, Y., Murai, T., Oishi, N., & Uchida, S. (2022). Antidepressant response and stress resilience are promoted by CART peptides in GABAergic neurons of the anterior cingulate cortex. *Biological Psychiatry Global Open Science*, 3(1), 87–98. <https://doi.org/10.1016/J.BPSGOS.2021.12.009>
- García-Moreno, F., Pedraza, M., Di Giovannantonio, L. G., Di Salvio, M., López-Mascaraque, L., Simeone, A., & De Carlos, J. A. (2010). A neuronal migratory pathway crossing from diencephalon to telencephalon populates amygdala nuclei. *Nature Neuroscience*, 13(6), 680–689. <https://doi.org/10.1038/NN.2556>
- Gascuel, J., Lemoine, A., Rigault, C., Datiche, F., Benani, A., Penicaud, L., & Lopez-Mascaraque, L. (2012). Hypothalamus-1 olfactory system crosstalk: Orexin A immunostaining in mice. *Frontiers in Neuroanatomy*, 6, 44. <https://doi.org/10.3389/FNANA.2012.00044>
- Gentier, R. J. G., Verheijen, B. M., Zamboni, M., Stroeken, M. M. A., Hermes, D. J. H. P., Küsters, B., Steinbusch, H. W. M., Hopkins, D. A., & Van Leeuwen, F. W. (2015). Localization of mutant ubiquitin in the brain of a transgenic mouse line with proteasomal inhibition and its validation at specific sites in Alzheimer's disease. *Frontiers in Neuroanatomy*, 9, 26. <https://doi.org/10.3389/fnana.2015.00026>
- Gutiérrez-Castellanos, N., Pardo-Bellver, C., Martínez-García, F., & Lanuza, E. (2014). The vomeronasal cortex—Afferent and efferent projections

- of the posteromedial cortical nucleus of the amygdala in mice. *European Journal of Neuroscience*, 39(1), 141–158. <https://doi.org/10.1111/EJN.12393>
- Gutzler, S. J., Karom, M., Erwin, W. D., & Albers, H. E. (2010). Arginine-vasopressin and the regulation of aggression in female Syrian hamsters (*Mesocricetus auratus*). *The European Journal of Neuroscience*, 31(9), 1655–1663. <https://doi.org/10.1111/J.1460-9568.2010.07190.X>
- Halasz, J., Zelena, D., Toth, M., Tulogdi, A., Mikics, E., & Haller, J. (2009). Substance P neurotransmission and violent aggression: The role of tachykinin NK(1) receptors in the hypothalamic attack area. *European Journal of Pharmacology*, 611(1–3), 35–43. <https://doi.org/10.1016/J.EJPHAR.2009.03.050>
- Hallem, E. A., & Carlson, J. R. (2006). Coding of odors by a receptor repertoire. *Cell*, 125(1), 143–160. <https://doi.org/10.1016/j.cell.2006.01.050>
- Heavner, W. E., Ji, S., Notwell, J. H., Dyer, E. S., Tseng, A. M., Birgmeier, J., Yoo, B., Bejerano, G., & McConnell, S. K. (2020). Transcription factor expression defines subclasses of developing projection neurons highly similar to single-cell RNA-seq subtypes. *Proceedings of the National Academy of Sciences of the United States of America*, 117(40), 25074–25084. <https://doi.org/10.1073/PNAS.2008013117>
- Henkel, B., Bintig, W., Bhat, S. S., Spehr, M., & Neuhaus, E. M. (2017). NHERF1 in microvilli of vomeronasal sensory neurons. *Chemical Senses*, 42(1), 25–35. <https://doi.org/10.1093/CHEMSE/BJW094>
- Herrada, G., & Dulac, C. (1997). A novel family of putative pheromone receptors in mammals with a topographically organized and sexually dimorphic distribution. *Cell*, 90(4), 763–773. [https://doi.org/10.1016/S0092-8674\(00\)80536-X](https://doi.org/10.1016/S0092-8674(00)80536-X)
- Herrero, M. J., Wang, L., Hernandez-Pineda, D., Banerjee, P., Matos, H. Y., Goodrich, M., Panigrahi, A., Smith, N. A., & Corbin, J. G. (2021). Sex-specific social behavior and amygdala proteomic deficits in Foxp2 +/- mutant mice. *Frontiers in Behavioral Neuroscience*, 15, 706079. <https://doi.org/10.3389/FNBEH.2021.706079>
- Hines, M., Allen, L. S., & Gorski, R. A. (1992). Sex differences in subregions of the medial nucleus of the amygdala and the bed nucleus of the stria terminalis of the rat. *Brain Research*, 579(2), 321–326. [https://doi.org/10.1016/0006-8993\(92\)90068-K](https://doi.org/10.1016/0006-8993(92)90068-K)
- Hintiryan, H., Atlas, O. D., Gou, H. H. L., Zingg, B., Yamashita, S., Lyden, H. M., Song, M. Y., Grewal, A. K., Zhang, X., Toga, A. W., & Dong, H. W. (2012). Comprehensive connectivity of the mouse main olfactory bulb: Analysis and online digital atlas. *Frontiers in Neuroanatomy*, 6, 30. <https://doi.org/10.3389/fnana.2012.00030>
- Hirata, T., Li, P., Lanuza, G. M., Cocas, L. A., Huntsman, M. M., & Corbin, J. G. (2009). Identification of distinct telencephalic progenitor pools for neuronal diversity in the amygdala. *Nature Neuroscience*, 12(2), 141–149. <https://doi.org/10.1038/nn.2241>
- Hörmann, N., Schilling, T., Ali, A. H., Serbe, E., Mayer, C., Borst, A., & Pujol-Martí, J. (2020). A combinatorial code of transcription factors specifies subtypes of visual motion-sensing neurons in *Drosophila*. *Development*, 147(9), dev186296. <https://doi.org/10.1242/DEV.186296>
- Huilgol, D., Udin, S., Shimogori, T., Saha, B., Roy, A., Aizawa, S., Hevner, R. F., Meyer, G., Ohshima, T., Pleasure, S. J., Zhao, Y., & Tole, S. (2013). Dual origins of the mammalian accessory olfactory bulb revealed by an evolutionarily conserved migratory stream. *Nature Neuroscience*, 16(2), 157–165. <https://doi.org/10.1038/nn.3297>
- Ichikawa, M., Takami, S., Osada, T., & Graziadei, P. P. C. (1994). Differential development of binding sites of two lectins in the vomeronasal axons of the rat accessory olfactory bulb. *Developmental Brain Research*, 78(1), 1–9. [https://doi.org/10.1016/0165-3806\(94\)90002-7](https://doi.org/10.1016/0165-3806(94)90002-7)
- Igarashi, K. M., Ieki, N., An, M., Yamaguchi, Y., Nagayama, S., Kobayakawa, K., Kobayakawa, R., Tanifuji, M., Sakano, H., Chen, W. R., & Mori, K. (2012). Parallel mitral and tufted cell pathways route distinct odor information to different targets in the olfactory cortex. *The Journal of Neuroscience*, 32(23), 7970–7985. <https://doi.org/10.1523/JNEUROSCI.0154-12.2012>
- Imamura, K., Mori, K., Fujita, S. C., & Obata, K. (1985). Immunohistochemical identification of subgroups of vomeronasal nerve fibers and their segregated terminations in the accessory olfactory bulb. *Brain Research*, 328(2), 362–366. [https://doi.org/10.1016/0006-8993\(85\)91050-9](https://doi.org/10.1016/0006-8993(85)91050-9)
- Isogai, Y., Si, S., Pont-Lezica, L., Tan, T., Kapoor, V., Murthy, V. N., & Dulac, C. (2011). Molecular organization of vomeronasal chemoreception. *Nature*, 478(7368), 241–245. <https://doi.org/10.1038/NATURE10437>
- Jia, C., & Halpern, M. (1996). Subclasses of vomeronasal receptor neurons: Differential expression of G proteins (*Gia2* and *Goa*) and segregated projections to the accessory olfactory bulb. *Brain Research*, 719(1–2), 117–128. [https://doi.org/10.1016/0006-8993\(96\)00110-2](https://doi.org/10.1016/0006-8993(96)00110-2)
- Kaczmarek-Hajek, K., Zhang, J., Kopp, R., Grosche, A., Rissiek, B., Saul, A., Bruzzone, S., Engel, T., Jooss, T., Krautloher, A., Schuster, S., Magnus, T., Stadelmann, C., Sirko, S., Nolte, F. K., Eulenburg, V., & Nicke, A. (2018). Re-evaluation of neuronal P2x7 expression using novel mouse models and a P2x7-specific nanobody. *eLife*, 7, e36217. <https://doi.org/10.7554/ELIFE.36217>
- Kang, N., Baum, M. J., & Cherry, J. A. (2011). Different profiles of main and accessory olfactory bulb mitral/tufted cell projections revealed in mice using an anterograde tracer and a whole-mount, flattened cortex preparation. *Chemical Senses*, 36(3), 251–260. <https://doi.org/10.1093/CHEMSE/BJQ120>
- Kang, N., McCarthy, E. A., Cherry, J. A., & Baum, M. J. (2011). A sex comparison of the anatomy and function of the main olfactory bulb-medial amygdala projection in mice. *Neuroscience*, 172, 196–204. <https://doi.org/10.1016/J.NEUROSCIENCE.2010.11.003>
- Karl, T., Lin, S., Schwarzer, C., Sainsbury, A., Couzens, M., Wittmann, W., Boey, D., Von Hörsten, S., & Herzog, H. (2004). Y1 receptors regulate aggressive behavior by modulating serotonin pathways. *Proceedings of the National Academy of Sciences of the United States of America*, 101(34), 12742–12747. <https://doi.org/10.1073/pnas.0404085101>
- Kast, R. J., Lanjewar, A. L., Smith, C. D., & Levitt, P. (2019). FOXP2 exhibits projection neuron class specific expression, but is not required for multiple aspects of cortical histogenesis. *eLife*, 8, e42012. <https://doi.org/10.7554/ELIFE.42012>
- Katrantha, S. M., Shaw, J. E., Zhao, A. Y., Myers, S. A., Cocco, A. R., Jeng, A. T., Zhu, M., Pittenger, C., Greer, C. A., Carr, S. A., Xiao, X., & Koleske, A. J. (2019). Trio haploinsufficiency causes neurodevelopmental disease-associated deficits. *Cell Reports*, 26(10), 2805.e9–2817.e9. <https://doi.org/10.1016/J.CELREP.2019.02.022>
- Katreddi, R. R., & Forni, P. E. (2021). Mechanisms underlying pre- and postnatal development of the vomeronasal organ. *Cellular and Molecular Life Sciences*, 78(12), 5069–5082. <https://doi.org/10.1007/S00018-021-03829-3>
- Keshavarzi, S., Sullivan, R. K. P., Ianno, D. J., & Sah, P. (2014). Functional properties and projections of neurons in the medial amygdala. *The Journal of Neuroscience*, 34(26), 8699–8715. <https://doi.org/10.1523/JNEUROSCI.1176-14.2014>
- Kimchi, T., Xu, J., & Dulac, C. (2007). A functional circuit underlying male sexual behaviour in the female mouse brain. *Nature*, 448(7157), 1009–1014. <https://doi.org/10.1038/nature06089>
- Kirouac, G. J., Parsons, M. P., & Li, S. (2006). Innervation of the paraventricular nucleus of the thalamus from cocaine- and amphetamine-regulated transcript (CART) containing neurons of the hypothalamus. *The Journal of Comparative Neurology*, 497(2), 155–165. <https://doi.org/10.1002/CNE.20971>
- Knöll, B., Schmidt, H., Andrews, W., Guthrie, S., Pini, A., Sundaresan, V., & Drescher, U. (2003). On the topographic targeting of basal vomeronasal axons through Slit-mediated chemorepulsion. *Development*, 130(21), 5073–5082. <https://doi.org/10.1242/DEV.00726>
- Kondabolu, K., Doig, N. M., Ayeko, O., Khan, B., Torres, A., Calvigioni, D., Meletis, K., Koós, T., & Magill, P. J. (2023). A selective projection from the subthalamic nucleus to parvalbumin-expressing interneurons of the striatum. *eNeuro*, 10(7), Article ENEURO.0417–21.2023. <https://doi.org/10.1523/ENEURO.0417-21.2023>

- Koolhaas, J. M., van den Brink, T. H. C., Roozendaal, B., & Boersma, F. (1990). Medial amygdala and aggressive behavior: Interaction between testosterone and vasopressin. *Aggressive Behavior*, 16, 223–229. [https://doi.org/10.1002/1098-2337\(1990\)16:3/4<223::AID-AB2480160308>3.0.CO;2-%23](https://doi.org/10.1002/1098-2337(1990)16:3/4<223::AID-AB2480160308>3.0.CO;2-%23)
- Kristensen, P., Judge, M. E., Thim, L., Ribel, U., Christjansen, K. N., Wulff, B. S., Clausen, J. T., Jensen, P. B., Madsen, O. D., Vrang, N., Larsen, P. J., & Hastrup, S. (1998). Hypothalamic CART is a new anorectic peptide regulated by leptin. *Nature*, 393(6680), 72–76. <https://doi.org/10.1038/29993>
- Kumar, A., Dudley, C. A., & Moss, R. L. (1999). Functional dichotomy within the vomeronasal system: Distinct zones of neuronal activity in the accessory olfactory bulb correlate with sex-specific behaviors. *The Journal of Neuroscience*, 19(20), RC32. <https://doi.org/10.1523/JNEUROSCI.19-20-J0003.1999>
- Kuteeva, E., Calza, L., Holmberg, K., Theodorsson, E., Ögren, S. O., & Hökfelt, T. (2004). Distribution of galanin and galanin transcript in the brain of a galanin-overexpressing transgenic mouse. *Journal of Chemical Neuroanatomy*, 28(4), 185–216. <https://doi.org/10.1016/j.jchemneu.2004.06.004>
- Kwon, J. T., Ryu, C., Lee, H., Sheffield, A., Fan, J., Cho, D. H., Bigler, S., Sullivan, H. A., Choe, H. K., Wickersham, I. R., Heiman, M., & Choi, G. B. (2021). An amygdala circuit that suppresses social engagement. *Nature*, 593(7857), 114–118. <https://doi.org/10.1038/s41586-021-03413-6>
- Larriva-Sahd, J. (2008). The accessory olfactory bulb in the adult rat: A cytological study of its cell types, neuropil, neuronal modules, and interactions with the main olfactory system. *The Journal of Comparative Neurology*, 510(3), 309–350. <https://doi.org/10.1002/CNE.21790>
- Lau, Y. E., & Cherry, J. A. (2000). Distribution of PDE4A and G(o) alpha immunoreactivity in the accessory olfactory system of the mouse. *Neuroreport*, 11(1), 27–32. <https://doi.org/10.1097/00001756-200001170-00006>
- Lee, S. J., Krieger, J. P., Vergara, M., Quinn, D., McDougale, M., de Araujo, A., Darling, R., Zollinger, B., Anderson, S., Pan, A., Simonnet, E. J., Pignatosa, A., Arnold, M., Singh, A., Langhans, W., Raybould, H. E., & de Lartigue, G. (2020). Blunted vagal cocaine- and amphetamine-regulated transcript promotes hyperphagia and weight gain. *Cell Reports*, 30(6), 2028.e4–2039.e4. <https://doi.org/10.1016/j.CELREP.2020.01.045>
- Lee, W., Dworz, M. F., Milewski, T. M., Champagne, F. A., & Curley, J. P. (2022). Social status mediated variation in hypothalamic transcriptional profiles of male mice. *Hormones and Behavior*, 142, 105176. <https://doi.org/10.1016/j.YHBEH.2022.105176>
- Lein, E. S., Hawrylycz, M. J., Ao, N., Ayres, M., Bensinger, A., Bernard, A., Boe, A. F., Boguski, M. S., Brockway, K. S., Byrnes, E. J., Chen, L., Chen, L., Chen, T. M., Chin, M. C., Chong, J., Crook, B. E., Czaplinska, A., Dang, C. N., Datta, S., ... Jones, A. R. (2006). Genome-wide atlas of gene expression in the adult mouse brain. *Nature*, 445(7124), 168–176. <https://doi.org/10.1038/nature05453>
- Li, X., Zhang, J., Li, D., He, C., He, K., Xue, T., Wan, L., Zhang, C., & Liu, Q. (2021). Astrocytic ApoE reprograms neuronal cholesterol metabolism and histone-acetylation-mediated memory. *Neuron*, 109(6), 957.e8–970.e8. <https://doi.org/10.1016/j.NEURON.2021.01.005>
- Li, Y., Bao, H., Luo, Y., Yoan, C., Sullivan, H. A., Quintanilla, L., Wickersham, I., Lazarus, M., Shih, Y. Y. I., & Song, J. (2020). Supramammillary nucleus synchronizes with dentate gyrus to regulate spatial memory retrieval through glutamate release. *eLife*, 9, e53129. <https://doi.org/10.7554/ELIFE.53129>
- Li, Y., & Dulac, C. (2018). Neural coding of sex-specific social information in the mouse brain. *Current Opinion in Neurobiology*, 53, 120–130. <https://doi.org/10.1016/j.CONB.2018.07.005>
- Li, Y., Mathis, A., Grewe, B. F., Osterhout, J. A., Ahanonu, B., Schnitzer, M. J., Murthy, V. N., & Dulac, C. (2017). Neuronal representation of social information in the medial amygdala of awake behaving mice. *Cell*, 171(5), 1176.e17–1190.e17. <https://doi.org/10.1016/j.cell.2017.10.015>
- Lischinsky, J. E., Sokolowski, K., Li, P., Esumi, S., Kamal, Y., Goodrich, M., Oboti, L., Hammond, T. R., Krishnamoorthy, M., Feldman, D., Huntsman, M., Liu, J., & Corbin, J. G. (2017). Embryonic transcription factor expression in mice predicts medial amygdala neuronal identity and sex-specific responses to innate behavioral cues. *eLife*, 6, e21012. <https://doi.org/10.7554/ELIFE.21012>
- Lischinsky, J. E., Yin, L., Shi, C., Prakash, N., Burke, J., Shekaran, G., Grba, M., Corbin, J. G., & Lin, D. (2023). Hardwired to attack: Transcriptionally defined amygdala subpopulations play distinct roles in innate social behaviors. *Nature Neuroscience*, <https://doi.org/10.1101/2023.03.16.532692>
- Liu, C., Lee, C. Y., Asher, G., Cao, L., Terakoshi, Y., Cao, P., Kobayakawa, R., Kobayakawa, K., Sakurai, K., & Liu, Q. (2021). Posterior subthalamic nucleus (PSTh) mediates innate fear-associated hypothermia in mice. *Nature Communications*, 12, 2648. <https://doi.org/10.1038/s41467-021-22914-6>
- Ma, L., Qiu, Q., Gradwohl, S., Scott, A., Yu, E. Q., Alexander, R., Wiegraebe, W., & Yu, C. R. (2012). Distributed representation of chemical features and tunotopic organization of glomeruli in the mouse olfactory bulb. *Proceedings of the National Academy of Sciences of the United States of America*, 109(14), 5481–5486. <https://doi.org/10.1073/PNAS.1117491109>
- Madeira, N., Drumond, A., & Fonseca, R. (2020). Temporal gating of synaptic competition in the amygdala by cannabinoid receptor activation. *Cerebral Cortex*, 30(7), 4064–4075. <https://doi.org/10.1093/CERCOR/BHAA026>
- Martin, C. B. P., Ramond, F., Farrington, D. T., Aguiar, A. S., Chevarin, C., Berthiau, A. S., Caussanel, S., Lanfumey, L., Herrick-Davis, K., Hamon, M., Madjar, J. J., & Mongeau, R. (2012). RNA splicing and editing modulation of 5-HT_{2C} receptor function: Relevance to anxiety and aggression in VGV mice. *Molecular Psychiatry*, 18(6), 656–665. <https://doi.org/10.1038/mp.2012.171>
- Matos, H. Y., Hernandez-Pineda, D., Charpentier, C. M., Rusk, A., Corbin, J. G., & Jones, K. S. (2020). Sex differences in biophysical signatures across molecularly defined medial amygdala neuronal subpopulations. *eNeuro*, 7(4), Article ENEURO.0035-20.2020. <https://doi.org/10.1523/ENEURO.0035-20.2020>
- Matsunami, H., & Buck, L. B. (1997). A multigene family encoding a diverse array of putative pheromone receptors in mammals. *Cell*, 90(4), 775–784. [https://doi.org/10.1016/S0092-8674\(00\)80537-1](https://doi.org/10.1016/S0092-8674(00)80537-1)
- Mayer, C., Hafemeister, C., Bandler, R. C., Machold, R., Batista Brito, R., Jaglin, X., Allaway, K., Butler, A., Fishell, G., & Satija, R. (2018). Developmental diversification of cortical inhibitory interneurons. *Nature*, 555(7697), 457–462. <https://doi.org/10.1038/NATURE25999>
- Medina, L., Legaz, I., González, G., De Castro, F., Rubenstein, J. L. R., & Puelles, L. (2004). Expression of Dbx1, Neurogenin 2, Semaphorin 5A, Cadherin 8, and Emx1 distinguish ventral and lateral pallial histogenetic divisions in the developing mouse claustroramygdaloid complex. *The Journal of Comparative Neurology*, 474(4), 504–523. <https://doi.org/10.1002/CNE.20141>
- Meurisse, M., Chaillou, E., & Lévy, F. (2009). Afferent and efferent connections of the cortical and medial nuclei of the amygdala in sheep. *Journal of Chemical Neuroanatomy*, 37(2), 87–97. <https://doi.org/10.1016/j.JCHEMNEU.2008.09.001>
- Mi, D., Li, Z., Lim, L., Li, M., Moissidis, M., Yang, Y., Gao, T., Hu, T. X., Pratt, T., Price, D. J., Sestan, N., & Marín, O. (2018). Early emergence of cortical interneuron diversity in the mouse embryo. *Science*, 360(6384), 81–85. <https://doi.org/10.1126/SCIENCE.AAR6821>
- Modol, L., Bollmann, Y., Tressard, T., Baude, A., Che, A., Duan, Z. R. S., Babij, R., De Marco García, N. V., & Cossart, R. (2020). Assemblies of perisomatic GABAergic neurons in the developing barrel cortex. *Neuron*, 105(1), 93.e4–105.e4. <https://doi.org/10.1016/j.NEURON.2019.10.007>
- Mombaerts, P., Wang, F., Dulac, C., Chao, S. K., Nemes, A., Mendelsohn, M., Edmondson, J., & Axel, R. (1996). Visualizing an olfactory sensory map. *Cell*, 87(4), 675–686. [https://doi.org/10.1016/S0092-8674\(00\)81387-2](https://doi.org/10.1016/S0092-8674(00)81387-2)
- Montani, G., Tonelli, S., Sanghez, V., Ferrari, P. F., Palanza, P., Zimmer, A., & Tirindelli, R. (2013). Aggressive behaviour and physiological responses

- to pheromones are strongly impaired in mice deficient for the olfactory G-protein γ -subunit Gy8. *The Journal of Physiology*, 591(16), 3949–3962. <https://doi.org/10.1113/JPHYSIOL.2012.247528>
- Münch, J., Billig, G., Hübner, C. A., Leinders-Zufall, T., Zufall, F., & Jentsch, T. J. (2018). Ca²⁺-activated Cl currents in the murine vomeronasal organ enhance neuronal spiking but are dispensable for male-male aggression. *Journal of Biological Chemistry*, 26, 10392–10403. <https://doi.org/10.1074/jbc.RA118.003153>
- Murakami, M., Kashiwadani, H., Kirino, Y., & Mori, K. (2005). State-dependent sensory gating in olfactory cortex. *Neuron*, 46(2), 285–296. <https://doi.org/10.1016/j.neuron.2005.02.025>
- Muroi, Y., & Ishii, T. (2015). Neuropeptide Y is crucial for nutritional state-dependent regulation of maternal behavior. *Psychoneuroendocrinology*, 51, 392–402. <https://doi.org/10.1016/j.psyneuen.2014.09.022>
- Nagayama, S., Homma, R., & Imamura, F. (2014). Neuronal organization of olfactory bulb circuits. *Frontiers in Neural Circuits*, 8, 98. <https://doi.org/10.3389/fncir.2014.00098>
- Nakamura, Y., Jörg, D. J., Kon, Y., Simons, B. D., & Yoshida, S. (2021). Transient suppression of transplanted spermatogonial stem cell differentiation restores fertility in mice. *Cell Stem Cell*, 28(8), 1443.e7–1456.e7. <https://doi.org/10.1016/j.stem.2021.03.016>
- Nara, K., Saraiva, L. R., Ye, X., & Buck, L. B. (2011). A large-scale analysis of odor coding in the olfactory epithelium. *Journal of Neuroscience*, 31(25), 9179–9191. <https://doi.org/10.1523/JNEUROSCI.1282-11.2011>
- Nguyen, U. P., & Imamura, F. (2019). Regional differences in mitral cell development in mouse olfactory bulb. *The Journal of Comparative Neurology*, 527(14), 2233–2244. <https://doi.org/10.1002/cne.24683>
- Nunez-Parra, A., Pugh, V., & Araneda, R. C. (2011). Regulation of adult neurogenesis by behavior and age in the accessory olfactory bulb. *Molecular and Cellular Neurosciences*, 47(4), 274–285. <https://doi.org/10.1016/j.mcn.2011.05.003>
- Oka, Y., Katada, S., Omura, M., Suwa, M., Yoshihara, Y., & Touhara, K. (2006). Odorant receptor map in the mouse olfactory bulb: In vivo sensitivity and specificity of receptor-defined glomeruli. *Neuron*, 52(5), 857–869. <https://doi.org/10.1016/j.neuron.2006.10.019>
- Padilla, S. L., Qiu, J., Soden, M. E., Sanz, E., Nestor, C. C., Barker, F. D., Quintana, A., Zweifel, L. S., Rønnekleiv, O. K., Kelly, M. J., & Palmiter, R. D. (2016). AgRP neural circuits mediate adaptive behaviors in the starved state. *Nature Neuroscience*, 19(5), 734–741. <https://doi.org/10.1038/nn.4274>
- Papes, F., Logan, D. W., & Stowers, L. (2010). The vomeronasal organ mediates interspecies defensive behaviors through detection of protein pheromone homologs. *Cell*, 141(4), 692–703. <https://doi.org/10.1016/j.cell.2010.03.037>
- Pardo-Bellver, C., Cádiz-Moretti, B., Novejarque, A., Martínez-García, F., & Lanuza, E. (2012). Differential efferent projections of the anterior, posterodorsal, and posterodorsal subdivisions of the medial amygdala in mice. *Frontiers in Neuroanatomy*, 6, 33. <https://doi.org/10.3389/fnana.2012.00033>
- Pro-Sistiaga, P., Mohedano-Moriano, A., Ubeda-Bañon, I., Del Mar Arroyo-Jimenez, M., Marcos, P., Artacho-Pérula, E., Crespo, C., Insausti, R., & Martínez-Marcos, A. (2007). Convergence of olfactory and vomeronasal projections in the rat basal telencephalon. *The Journal of Comparative Neurology*, 504(4), 346–362. <https://doi.org/10.1002/cne.21455>
- Puciklowski, O., Trzaskowska, E., Kostowski, W., & Wośko, W. (1988). Inhibition of affective aggression and dominance in rats after thyrotropin-releasing hormone (TRH) microinjection into the nucleus accumbens. *Peptides*, 9(3), 539–543. [https://doi.org/10.1016/0196-9781\(88\)90161-1](https://doi.org/10.1016/0196-9781(88)90161-1)
- Reimers-Kipping, S., Hevers, W., Pääbo, S., & Enard, W. (2011). Humanized Foxp2 specifically affects cortico-basal ganglia circuits. *Neuroscience*, 175, 75–84. <https://doi.org/10.1016/j.neuroscience.2010.11.042>
- Rigney, N., Whylings, J., Mieda, M., De Vries, G. J., & Petrulevicius, A. (2019). Sexually dimorphic vasopressin cells modulate social investigation and communication in sex-specific ways. *eNeuro*, 6(1), Article ENEURO.0415-18.2019. <https://doi.org/10.1523/ENEURO.0415-18.2019>
- Rouso, D. L., Qiao, M., Kagan, R. D., Yamagata, M., Palmiter, R. D., & Sanes, J. R. (2016). Two pairs of ON and OFF retinal ganglion cells are defined by intersectional patterns of transcription factor expression. *Cell Reports*, 15(9), 1930–1944. <https://doi.org/10.1016/j.celrep.2016.04.069>
- Rubin, B. D., & Katz, L. C. (1999). Optical imaging of odorant representations in the mammalian olfactory bulb. *Neuron*, 23(3), 499–511. [https://doi.org/10.1016/S0896-6273\(00\)80803-X](https://doi.org/10.1016/S0896-6273(00)80803-X)
- Ruiz Tejada Segura, M. L., Abou Moussa, E., Garabello, E., Nakahara, T. S., Makhoulouf, M., Mathew, L. S., Wang, L., Valle, F., Huang, S. S. Y., Mainland, J. D., Caselle, M., Osella, M., Lorenz, S., Reisert, J., Logan, D. W., Malnic, B., Scialdone, A., & Saraiva, L. R. (2022). A 3D transcriptomics atlas of the mouse nose sheds light on the anatomical logic of smell. *Cell Reports*, 38(12), 110547. <https://doi.org/10.1016/j.celrep.2022.110547>
- Ryba, N. J. P., & Tirindelli, R. (1997). A new multigene family of putative pheromone receptors. *Neuron*, 19(2), 371–379. [https://doi.org/10.1016/S0896-6273\(00\)80946-0](https://doi.org/10.1016/S0896-6273(00)80946-0)
- Sagner, A., Zhang, I., Watson, T., Lazaro, J., Melchionda, M., & Briscoe, J. (2021). A shared transcriptional code orchestrates temporal patterning of the central nervous system. *PLoS Biology*, 19(11), e3001450. <https://doi.org/10.1371/JOURNAL.PBIO.3001450>
- Sajdyk, T. J., Schober, D. A., Smiley, D. L., & Gehlert, D. R. (2002). Neuropeptide Y-Y2 receptors mediate anxiety in the amygdala. *Pharmacology Biochemistry and Behavior*, 71(3), 419–423. [https://doi.org/10.1016/S0091-3057\(01\)00679-7](https://doi.org/10.1016/S0091-3057(01)00679-7)
- Sajdyk, T. J., Vandergriff, M. G., & Gehlert, D. R. (1999). Amygdalar neuropeptide Y Y1 receptors mediate the anxiolytic-like actions of neuropeptide Y in the social interaction test. *European Journal of Pharmacology*, 368(2–3), 143–147. [https://doi.org/10.1016/S0014-2999\(99\)00018-7](https://doi.org/10.1016/S0014-2999(99)00018-7)
- Sakano, H. (2010). Neural map formation in the mouse olfactory system. *Neuron*, 67(4), 530–542. <https://doi.org/10.1016/j.neuron.2010.07.003>
- Sammoura, F. M., Popova, D., Morris, A., Hart, R. P., & Richardson, J. R. (2023). Methods for shipping live primary cortical and hippocampal neuron cultures from postnatal mice. *Current Research in Neurobiology*, 4, 100069. <https://doi.org/10.1016/j.crneur.2022.100069>
- Saunders, A., Johnson, C. A., & Sabatini, B. L. (2012). Novel recombinant adeno-associated viruses for Cre activated and inactivated transgene expression in neurons. *Frontiers in Neural Circuits*, 6, 47. <https://doi.org/10.3389/fncir.2012.00047>
- Schindelin, J., Arganda-Carreras, I., Frise, E., Kaynig, V., Longair, M., Pietzsch, T., Preibisch, S., Rueden, C., Saalfeld, S., Schmid, B., Tinevez, J.-Y., White, D. J., Hartenstein, V., Eliceiri, K., Tomancak, P., & Cardona, A. (2012). Fiji: An open-source platform for biological-image analysis. *Nature Methods*, 9(7), 676–682. <https://doi.org/10.1038/nmeth.2019>
- Séjourné, J., Llana, D., Kuti, O. J., & Page, D. T. (2015). Social behavioral deficits coincide with the onset of seizure susceptibility in mice lacking serotonin receptor 2c. *PLoS ONE*, 10(8), e0136494. <https://doi.org/10.1371/JOURNAL.PONE.0136494>
- Shemesh, Y., Forkosh, O., Mahn, M., Anpilov, S., Sztainberg, Y., Manashirov, S., Shlapobersky, T., Elliott, E., Tabouy, L., Ezra, G., Adler, E. S., Ben-Efraim, Y. J., Gil, S., Kuperman, Y., Haramati, S., Dine, J., Eder, M., Deussing, J. M., Schneidman, E., ... Chen, A. (2016). Ucn3 and CRF-R2 in the medial amygdala regulate complex social dynamics. *Nature Neuroscience*, 19(11), 1489–1496. <https://doi.org/10.1038/nn.4346>
- Shepherd, G. M. (2005). Perception without a thalamus: How does olfaction do it? *Neuron*, 46(2), 166–168. <https://doi.org/10.1016/j.neuron.2005.03.012>
- Shiple, M. T., & Adamek, G. D. (1984). The connections of the mouse olfactory bulb: A study using orthograde and retrograde transport of wheat germ agglutinin conjugated to horseradish peroxidase. *Brain Research Bulletin*, 12(6), 669–688. [https://doi.org/10.1016/0361-9230\(84\)90148-5](https://doi.org/10.1016/0361-9230(84)90148-5)
- Simerly, R. B. (2003). Wired for reproduction: Organization and development of sexually dimorphic circuits in the mammalian forebrain.

- Annual Review of Neuroscience*, 25, 507–536. <https://doi.org/10.1146/ANNUREV.NEURO.25.112701.142745>
- Stanic, D., Brumovsky, P., Fetissov, S., Shuster, S., Herzog, H., & Hokfelt, T. (2006). Characterization of neuropeptide Y2 receptor protein expression in the mouse brain. I. Distribution in cell bodies and nerve terminals. *The Journal of Comparative Neurology*, 499, 357–390. <https://doi.org/10.1002/cne.21046>
- Stengel, A., & Taché, Y. (2014). CRF and urocortin peptides as modulators of energy balance and feeding behavior during stress. *Frontiers in Neuroscience*, 8, 52. <https://doi.org/10.3389/FNINS.2014.00052>
- Stowers, L., Holy, T. E., Meister, M., Dulac, C., & Koentges, G. (2002). Loss of sex discrimination and male-male aggression in mice deficient for TRP2. *Science*, 295(5559), 1493–1500. <https://doi.org/10.1126/SCIENCE.1069259/>
- Stowers, L., & Liberles, S. D. (2016). State-dependent responses to sex pheromones in mouse. *Current Opinion in Neurobiology*, 38, 74–79. <https://doi.org/10.1016/J.CONB.2016.04.001>
- Sugai, T., Sugitani, M., & Onoda, N. (1999). Novel subdivisions of the rat accessory olfactory bulb revealed by the combined method with lectin histochemistry, electrophysiological and optical recordings. *Neuroscience*, 95(1), 23–32. [https://doi.org/10.1016/S0306-4522\(99\)00403-0](https://doi.org/10.1016/S0306-4522(99)00403-0)
- Terranova, J. I., Ferris, C. F., & Albers, H. E. (2017). Sex differences in the regulation of offensive aggression and dominance by arginine-vasopressin. *Frontiers in Endocrinology*, 8, 308. <https://doi.org/10.3389/FENDO.2017.00308>
- Tervo, D. G. R., Hwang, B. Y., Viswanathan, S., Gaj, T., Lavzin, M., Ritola, K. D., Lindo, S., Michael, S., Kuleshova, E., Ojala, D., Huang, C. C., Gerfen, C. R., Schiller, J., Dudman, J. T., Hantman, A. W., Looger, L. L., Schaffer, D. V., & Karpova, A. Y. (2016). A designer AAV variant permits efficient retrograde access to projection neurons. *Neuron*, 92(2), 372–382. <https://doi.org/10.1016/J.NEURON.2016.09.021>
- Thoß, M., Luzynski, K. C., Enk, V. M., Razzazi-Fazeli, E., Kwak, J., Ortner, I., & Penn, D. J. (2019). Regulation of volatile and non-volatile pheromone attractants depends upon male social status. *Scientific Reports*, 9, 489. <https://doi.org/10.1038/s41598-018-36887-y>
- Torz, L., Niss, K., Lundh, S., Rekling, J. C., Quintana, C. D., Emilie, S., Frazier, D., Mercer, A. J., Cornea, A., Bertelsen, C. V., Gerstenberg, M. K., Kruse Hansen, A. M., Guldbrandt, M., Lykkesfeldt, J., John, L. M., Villaescusa, J. C., & Petersen, N. (2022). NPFF decreases activity of human arcuate NPY neurons: A study in embryonic-stem-cell-derived model. *International Journal of Molecular Sciences*, 23(6), 3260. <https://doi.org/10.3390/ijms23063260>
- Treloar, H. B., Purcell, A. L., & Greer, C. A. (1999). Glomerular formation in the developing rat olfactory bulb. *The Journal of Comparative Neurology*, 413(2), 289–304. [https://doi.org/10.1002/\(SICI\)1096-9861\(19991018\)413:2<289::AID-CNE9>3.0.CO;2-U](https://doi.org/10.1002/(SICI)1096-9861(19991018)413:2<289::AID-CNE9>3.0.CO;2-U)
- Uchida, N., Poo, C., & Haddad, R. (2014). Coding and transformations in the olfactory system. *Annual Review of Neuroscience*, 37, 363–385. <https://doi.org/10.1146/annurev-neuro-071013-013941>
- Vassar, R., Chao, S. K., Sitcheran, R., Nuñez, J. M., Vossahl, L. B., & Axel, R. (1994). Topographic organization of sensory projections to the olfactory bulb. *Cell*, 79(6), 981–991. [https://doi.org/10.1016/0092-8674\(94\)90029-9](https://doi.org/10.1016/0092-8674(94)90029-9)
- Wachowiak, M., & Cohen, L. B. (2001). Representation of odorants by receptor neuron input to the mouse olfactory bulb. *Neuron*, 32(4), 723–735. [https://doi.org/10.1016/S0896-6273\(01\)00506-2](https://doi.org/10.1016/S0896-6273(01)00506-2)
- Wagner, S., Gresser, A. L., Torello, A. T., & Dulac, C. (2006). A multireceptor genetic approach uncovers an ordered integration of VNO sensory inputs in the accessory olfactory bulb. *Neuron*, 50(5), 697–709. <https://doi.org/10.1016/J.NEURON.2006.04.033>
- Wang, C., Xiong, M., Gratuzze, M., Bao, X., Shi, Y., Andhey, P. S., Manis, M., Schroeder, C., Yin, Z., Madore, C., Butovsky, O., Artyomov, M., Ulrich, J. D., & Holtzman, D. M. (2021). Selective removal of astrocytic APOE4 strongly protects against tau-mediated neurodegeneration and decreases synaptic phagocytosis by microglia. *Neuron*, 109(10), 1657.e7–1674.e7. <https://doi.org/10.1016/J.NEURON.2021.03.024>
- Whyllings, J., Rigney, N., Peters, N. V., de Vries, G. J., & Petrulis, A. (2020). Sexually dimorphic role of BNST vasopressin cells in sickness and social behavior in male and female mice. *Brain, Behavior, and Immunity*, 83, 68–77. <https://doi.org/10.1016/J.BBI.2019.09.015>
- Wu, Y. E., Pan, L., Zuo, Y., Li, X., & Hong, W. (2017). Detecting activated cell populations using single-cell RNA-seq. *Neuron*, 96(2), 313.e6–329.e6. <https://doi.org/10.1016/j.neuron.2017.09.026>
- Wysocki, C. J., & Lepri, J. J. (1991). Consequences of removing the vomeronasal organ. *The Journal of Steroid Biochemistry and Molecular Biology*, 39(4B), 661–669. [https://doi.org/10.1016/0960-0760\(91\)90265-7](https://doi.org/10.1016/0960-0760(91)90265-7)
- Xu, X., Coats, J. K., Yang, C. F., Wang, A., Ahmed, O. M., Alvarado, M., Izumi, T., & Shah, N. M. (2012). Modular genetic control of sexually dimorphic behaviors. *Cell*, 148(3), 596–607. <https://doi.org/10.1016/J.CELL.2011.12.018>
- Yang, S.-T., Wang, M., Paspalas, C. D., Crimins, J. L., Altman, M. T., Mazer, J. A., & Arnsten, A. F. T. (2018). Core differences in synaptic signaling between primary visual and dorsolateral prefrontal cortex. *Cerebral Cortex*, 28, 1458–1471. <https://doi.org/10.1093/cercor/bhx357>
- Yao, S., Bergan, J., Lanjuin, A., & Dulac, C. (2017). Oxytocin signaling in the medial amygdala is required for sex discrimination of social cues. *eLife*, 6, e31373. <https://doi.org/10.7554/ELIFE.31373>
- Yin, L., Hashikawa, K., Hashikawa, Y., Osakada, T., Lischinsky, J. E., Diaz, V., & Lin, D. (2022). VMHvl^{Cckar} cells dynamically control female sexual behaviors over the reproductive cycle. *Neuron*, 110(18), 3000.e8–3017.e8. <https://doi.org/10.1016/J.NEURON.2022.06.026>
- Yonekura, J., & Yokoi, M. (2008). Conditional genetic labeling of mitral cells of the mouse accessory olfactory bulb to visualize the organization of their apical dendritic tufts. *Molecular and Cellular Neuroscience*, 37(4), 708–718. <https://doi.org/10.1016/J.MCN.2007.12.016>
- Zelikowsky, M., Hui, M., Karigo, T., Choe, A., Yang, B., Blanco, M. R., Beadle, K., Gradinaru, V., Deverman, B. E., & Anderson, D. J. (2018). The neuropeptide Tac2 controls a distributed brain state induced by chronic social isolation stress. *Cell*, 173(5), 1265.e19–1279.e19. <https://doi.org/10.1016/J.CELL.2018.03.037>
- Zeppilli, S., Ackels, T., Attey, R., Klimpert, N., Ritola, K. D., Boeing, S., Crombach, A., Schaefer, A. T., & Fleischmann, A. (2021). Molecular characterization of projection neuron subtypes in the mouse olfactory bulb. *eLife*, 10, e65445. <https://doi.org/10.7554/ELIFE.65445>
- Zhang, Z., Beier, C., Weil, T., & Hattar, S. (2021). The retinal ipRGC-preoptic circuit mediates the acute effect of light on sleep. *Nature Communications*, 12(1), 5115. <https://doi.org/10.1038/S41467-021-25378-W>
- Zheng, N., Wang, Z. Z., Wang, S. W., Yang, F. J., Zhu, X. T., Lu, C., Manyande, A., Rao, X. P., & Xu, F. Q. (2020). Co-localization of two-color rAAV2-retro confirms the dispersion characteristics of efferent projections of mitral cells in mouse accessory olfactory bulb. *Zoological Research*, 41(2), 148–156. <https://doi.org/10.24272/J.ISSN.2095-8137.2020.020>

How to cite this article: Prakash, N., Matos, H. Y., Sebaoui, S., Tsai, L., Tran, T., Aromolaran, A., Atrachji, I., Campbell, N., Goodrich, M., Hernandez-Pineda, D., Herrero, M. J., Hirata, T., Lischinsky, J., Martinez, W., Torii, S., Yamashita, S., Hosseini, H., Sokolowski, K., Esumi, S., ... Corbin, J. G. (2023). Connectivity and molecular profiles of *Foxp2*- and *Dbx1*-lineage neurons in the accessory olfactory bulb and medial amygdala. *Journal of Comparative Neurology*, 1–26. <https://doi.org/10.1002/cne.25545>